Desalination 550 (2023) 116374

Contents lists available at ScienceDirect

Desalination

journal homepage: www.elsevier.com/locate/desal

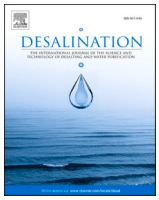

Potential application of hybrid reverse electrodialysis (RED)-forward osmosis (FO) system to fertilizer-producing industrial plant for efficient water reuse

Tasneem Elmakki [a], Sifani Zavahir [a], Mona Gulied [a], Hazim Qiblawey [b], Bassim Hammadi [b], Majeda Khraisheh [b], Ho Kyong Shon [c], Hyunwoong Park [d,*], Dong Suk Han [a,b,**]

[a] Center for Advanced Materials, Qatar University, Doha, Qatar
[b] Department of Chemical Engineering, College of Engineering, Qatar University, Doha, Qatar
[c] Faculty of Engineering and IT, Faculty of Engineering and IT, University of Technology, Sydney, P.O. Box 123, Broadway, NSW 2007, Australia
[d] School of Energy Engineering, Kyungpook National University, Daegu 41566, Republic of Korea

HIGHLIGHTS

- Reverse electrodialysis (RED)-forward osmosis (FO) hybrid system for wastewater reuse
- Highest power density of 2.17 W/m^2 at 0.015 M $(NH_4)_2SO_4$/1 M NaCl solution pair
- The most consistent power generation with 20 pairs of membrane cells in a single-pass flow mode
- RED effluent to a subsequent FO system as a draw solution (DS) was investigated.
- Dilution rate (17 %) and a conductivity (1–2 mS/cm of DS) suitable for agricultural fertigation application

ARTICLE INFO

Keywords:
Reverse electrodialysis (RED)
Forward osmosis (FO)
Blue energy
Water reuse
Agricultural fertigation
Fertilizer-producing industry
Reverse osmosis (RO) brine

ABSTRACT

This study presents an experimental investigation and a parametric analysis of the applicability of agricultural fertigation and power generation using a reverse electrodialysis-forward osmosis (RED-FO) hybrid system, with a water stream discharged from a fertilizer-producing plant. The results of this study demonstrated the possibility of achieving high salinity power generation from the RED system utilizing high-salinity brine and low-salinity ammonia solution that simulates reverse osmosis (RO) brine and wastewater streams released by the fertilizer-producing industry. The feasibility of stream dilution for fertigation application is demonstrated when the resulting moderately saline RED effluent is introduced into the FO process as a draw solution. The effect of external load addition, flow velocities variation, and concentration changes of the working solutions on the overall stack internal resistance and, thereby, RED performance was evaluated. As such, the lowest internal resistance converged to a threshold value of 4.03 Ω, giving the highest gross power density of 2.17 W/m^2 when a flow velocity of 1.18 cm/s, 10 Ω external load, and 0.015 M $(NH_4)_2SO_4$/1 M NaCl solution pair were utilized. In addition, the effect of the number of ion exchange membrane pairs and wastewater stream recycling was studied and optimized to amplify the osmotically generated power. As a result, the most consistent power generation was achieved when using 20 pairs of membrane cells in a single-pass flow mode operation. The applicability of the RED effluent to a subsequent FO system as a draw solution (DS) was investigated, showing a dilution rate (17 %) and a conductivity (1–2 mS/cm of DS) suitable for agricultural fertigation applications.

* Corresponding author.
** Correspondence to: D. S. Han, Center for Advanced Materials, Qatar University, Doha, Qatar.
E-mail addresses: hwp@knu.ac.kr (H. Park), dhan@qu.edu.qa (D.S. Han).

https://doi.org/10.1016/j.desal.2023.116374
Received 27 July 2022; Received in revised form 12 December 2022; Accepted 6 January 2023
Available online 14 January 2023

1. Introduction

Sustainable energy acquisition has become the primary target for meeting today's technological and process advances, particularly in regions strongly dependent on limited hydrocarbon fuel energy, such as the Gulf Cooperation Council (GCC) countries [1]. Moreover, the industrial plants associated with this fuel production are usually aligned with numerous waste liquid streams that require proper management to minimize the release of hazardous liquids into the sea. And with the poor soil quality and lack of irrigation water in these countries, the reclamation of all water sources for potential food production is of primary importance. Thus, finding sustainable solutions to address the aforementioned demands of sustainable energy acquisition, waste stream management, liquid discharge minimization, and water and food security is very much needed.

In the region focused on in this study, the sole source of clean drinkable water is seawater desalination processes, where seawater reverse osmosis (SWRO) accounts for >50 % of the total supply [2]. Reverse osmosis (RO) brine rejected by RO membrane as a function of % water recovery is a highly pressurized stream with a pressure of nearly 75 bars and is discharged with elevated salinity levels of around 63–70 g/L [3] if 3.5 wt% seawater is used [4]. In other words, this SWRO brine is highly pressurized saline water that can recover hydraulic and osmotic pressures and valuable elements. Energy recovery devices (ERD) using the isobaric technology to utilize the highly pressurized RO brine are the most efficient devices for such purpose and can recover up to 98 % of the energy from the brine waste stream [5]. Here, the high salt contents present in SWRO brine also have a high potential to be exploited by other treatment methods. One of these methods is to use the salinity gradient energy (called blue energy) developed when this high-salinity stream is combined with another low-salinity wastewater stream as an additional energy source.

The salinity gradient power (SGP) is obtained via exploring the Gibbs free energy available when mixing two aqueous solutions with different salt contents [6]. The global SGP potential is around 2.4–2.6 terawatts [7]. The retrieval of blue energy is less dependent on weather conditions. Thus, additional energy storage systems may not be required to support the uncertainty of the power supply. Moreover, since harnessing SGP produces only brackish water as a byproduct, significant physical/chemical changes in the natural environment are not expected when the effluent is disposed to the sea with a similar salinity.

Of the several technologies used to generate salinity gradient power, pressure retarded osmosis (PRO) and reverse electrodialysis (RED) are the most promising, both of which have reached a commercial level. The PRO converts the salinity gradient energy generated across a semi-permeable membrane into electrical power using a hydro-turbine. RED, on the other hand, is an electrochemical process that uses ion exchange membranes and electrodes, where the transport of ions across the ion exchange membranes produces an electrochemical potential that can be converted to electrical energy at the electrodes [8]. Over the last decade, both processes have been highly investigated, reaching the pilot scale, but compared to PRO, the power density of RED is lower in non-fouling conditions. However, through proper process optimization of operating parameters and cell design alteration, the calculated net power density is expected to be improved up to 20 W/m^2 or more. Also, the power density loss due to fouling is less in RED (0–11.2 %) than in PRO (14.2–58.7 %) [9]. Thus, combining RED with other processes will extend its outstanding benefits.

In recent years, several efforts have been raised to properly investigate the great potential that RED technology entails for renewable energy generation. Most of these efforts have been studied in lab-scale systems [10] and have been directed primarily towards investigating the influence of various operating variables [11–14] and modes of operation [15,16]. In addition, many studies have been focused on the optimization of the RED stack designs and configurations, including the material design and properties of ion-exchange membranes [14,17,18], spacers [19–21], and accompanying electrodes [22,23]. These RED operating variables and model design studies allowed for an appropriate assessment of the technology at hand and opened up the possibility of its integration with other processes to further extend its applications. Fig. 1 illustrates and summarizes the main focus of various recent RED studies, particularly highlighting the use of these studies in building up the baseline and extending them to hybrid RED technologies.

RED hybrid processes can be broadly classified into two system categories: Externally integrated processes (EIPs) and internally integrated processes (IIPs). Hybrid systems belonging to the EIPs segment include systems consisting of two or more individual processes combined together. Most documented work on these systems uses high salinity brine with seawater as the working fluids – high concentration (HC) solution and low concentration (LC) solution - in the RED system. For instance, Zhao et al. [24] used the RED system for industrial RO brine treatment and investigated the possibility of its integration with a pressure-driven desalination system. Other attempts include the integration of RED with electrochemically driven desalination processes such as capacitive deionization (CDI) [25] and electrodialysis (ED) [26], in which RED-CDI and RED-ED hybrid systems were evaluated as feasible and economically attractive. Some other hybrid systems incorporate thermally driven processes with the RED system. The integration of RED with a heat engine system to restore the salinity gradient of the working fluid was reported in the literature [27,28], and the potential of combining a heat-driven membrane distillation (MD) system with RED has also been investigated [29,30]. It is important to note that of those hybrid RED-EIPs systems, only Mercer's research [30] involved utilizing a wastewater source as a working fluid in a RED-MD hybrid system. This study used municipal wastewater as a working fluid against freshwater. Compared to hybrid RED-EIPs, hybrid RED-IIPs put a greater emphasis on wastewater streams, especially industrial ones. As shown in Fig. 1, published works on RED-IIPs reported that their system utilized multiple wastewater streams such as organic wastewater [31], aquaculture wastewater [32], dye wastewater [33,34], and sulfur-rich alkaline wastewater [35]. However, the treatment and use of those wastewaters were performed as part of the redox reaction in the anode and cathode chambers while using synthetic NaCl solution as the working fluid. Although some non-integrated bench-scale [36–38] and pilot-scale RED [39,40] systems have explored municipal wastewater and treated wastewater as working fluids, both integrated and non-integrated RED systems involved minimal exploration of ammonia-based wastewater, a particularly significant industrial wastewater stream. Ammonia-based wastewater, mostly discharged in large quantities from the fertilizer-producing industry, is usually denitrified to reduce excess nitrogen that could negatively impact water quality and the ecosystem. In this context, Zhou et al. [41] demonstrated an attempt to denitrify and decompose ammonia-based wastewater in a single RED redox chamber. Despite many efforts to treat ammonia wastewater, an alternative approach that dilutes and utilizes this wastewater for direct agricultural irrigation can provide significant potential. The nutritional value associated with ammonia-based wastewater lies in releasing nitrogen, a nutrient essential for growing plants and crops and soil fertility. Several studies [42,43] dedicated to analyzing ammonia-based wastewater for direct agricultural fertigation demonstrate this potential. Nevertheless, the analysis of this wastewater for use in blue energy generation and fertigation is still lacking.

Thus, this study aims to explore the potential of a novel hybrid RED-EIP using multiple industrial waste streams, including the high salinity SWRO brine and ammonia-based wastewater, for the simultaneous generation of electrical energy and fertilizer water in a reverse electrodialysis-forward osmosis (RED-FO) hybrid system. The system proposed here will generate blue energy in the RED system by continuously feeding SWRO brine as an HC solution against a continuous flow of LC solution fed from industrial ammonia-based wastewater. As a result, the process constantly generates power, and the resulting diluted brine stream from this mixing process is further diluted through a

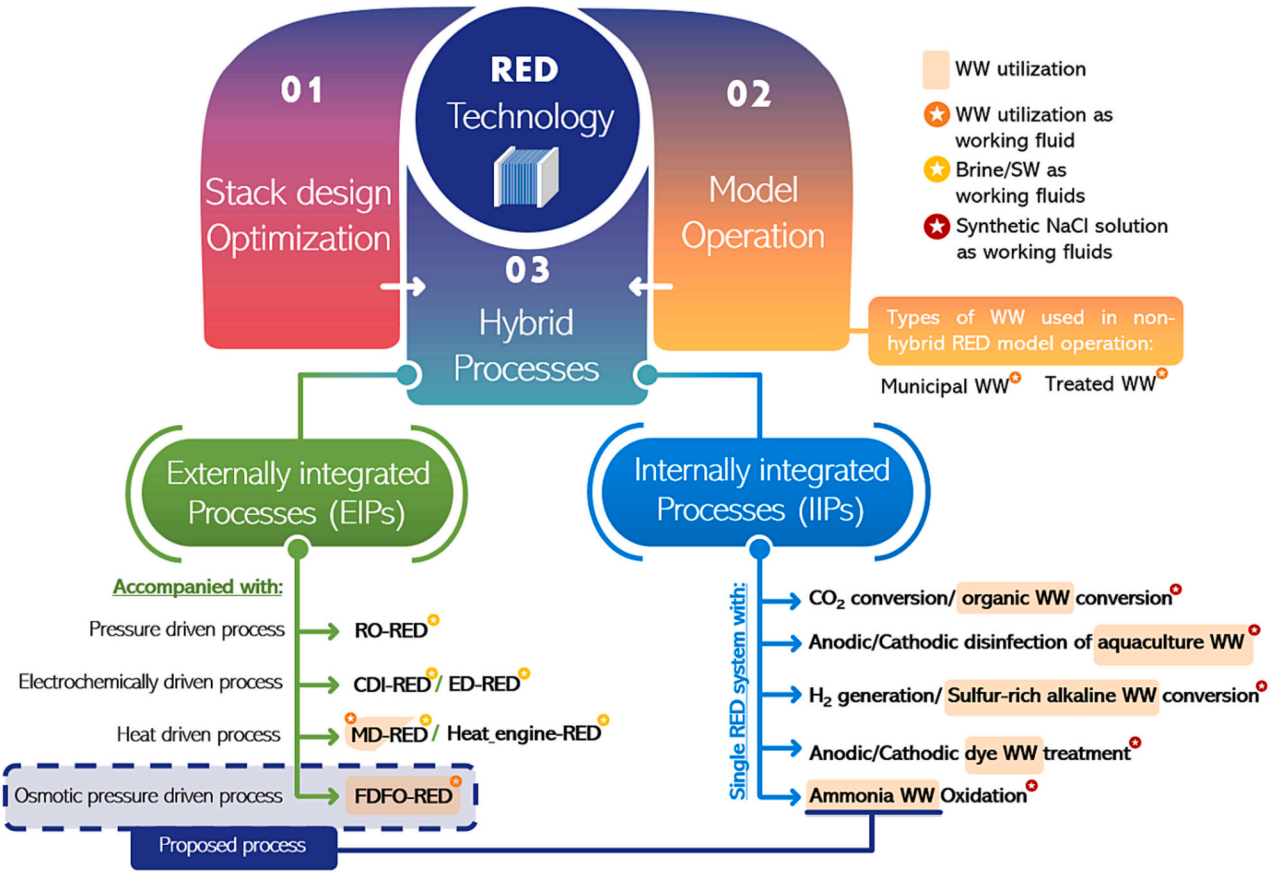

Fig. 1. The recent RED research focusing on existing RED hybrid processes and their wastewater utilization.

subsequent FO system and used for direct fertigation, increasing the sustainability of the process. In the FO process, the effluent of RED is applied as a draw solution (DS) against a relatively low salinity feed solution (FS). The FS to be used can be an industrial water stream, such as cooling water or process water. Most importantly, however, the stream must have a sufficiently low salinity to create an adequate osmotic pressure differential across the FO membrane, leading to a proper water transfer from the FS side to the DS side. A schematic illustrating the overall proposed process is presented in Fig. 2. Using the wasted industrial streams through the proposed process will, firstly, prevent the undesirable disposal of high salinity brine back into the sea, and secondly, prevent the wastage of ammonia-rich wastewater that can improve agricultural productivity.

In this work, synthetic solutions of SWRO brine (NaCl solution) and ammonia-based WW ($(NH_4)_2SO_4$) are used to examine the concept of the RED-FO hybrid system. However, in practice, both of these influent solutions have more complex compositions and involve various amounts of contaminants since they are essentially aqueous industrial effluents.

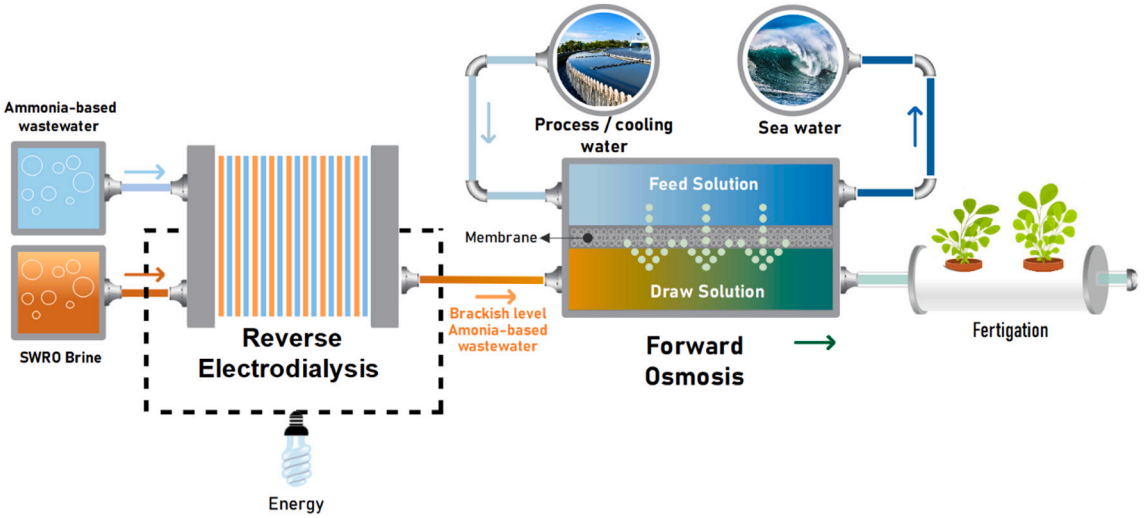

Fig. 2. Schematic diagram of the proposed reverse electrodialysis-forward osmosis (RED-FO) hybrid system for simultaneous production of electrical power and fertigation water, utilizing reverse osmosis (RO) brine and ammonia-based wastewater effluents.

These complex solution compositions may tremendously influence the subsequent proposed membrane-based technologies' performance. Hence, it is necessary to apply appropriate pretreatment methodologies to these streams.

Typical configurations for SWRO brine (HC solution) effluent industrial stream primarily include: (1) cations such as sodium (Na^+), magnesium (Mg^{2+}), calcium (Ca^{2+}), and potassium (K^+), (2) anions such as chloride (Cl^-), sulfate (SO_4^{2-}), and bicarbonate (HCO_3^-) [44], (3) trace metals such as barium (Ba), cesium (Cs), indium (In), iron (Fe), lead (Pb), and lithium (Li), and (4) numerous organic matter and contaminants [3]. The relatively complex composition of the SWRO brine significantly affects the performance of the RED system, which as essentially a membrane-based process. Several pilot-scale studies have shown that the use of natural seawater brine as HC drastically reduced the RED performance by up to 50 % compared to a synthetic solution containing only NaCl [40,45]. The performance degradation of the RED process is mainly related to divalent ions such as magnesium and calcium in the flowing stream. These divalent ions can (1) cause an uphill transport effect on the entire concentration gradient of the RED system, (2) increase the membrane resistance due to the binding of divalent cations inside the membranes [46], and (3) cause membrane fouling and scaling, blocking the membrane stack pores and henceforth reducing the ionic current responsible for power production in the RED cell [47]. In order to prevent performance degradation of RED, proper pretreatment such as ultrafiltration (UF) or dissolved air flotation (DAF) to remove organic matter is crucial [25]. According to Ju's study [48], the use of nanofiltration as a pretreatment of RO brine greatly improved power production in the RED process because it is the best in reducing the amount of divalent ions compared to other pretreatment technologies, such as cartridge filter, microfiltration, ultrafiltration, granular activated carbon, and activated filter media.

The nature of WW effluent streams from the chemical fertilizer industry varies in terms of composition and complexity. Hence, the WW treatment strategy requires thorough identification and application of suitable treatment methods based on the effluent's nature. WW from the chemical fertilizer industry mainly contains organic compounds, alcohols, ammonia, nitrates, and phosphorous, as well as heavy metals such as cadmium and suspended solids, contributing to increases in chemical oxygen demand (COD) (up to 140,000 ppm) and ammonia nitrogen (up to 1700 ppm) [49]. High COD in these streams indicates the presence of organic contaminants on the membranes of the RED system that cause significant biofouling. Industrial WW can be pretreated in several ways to remove COD, including coagulation, adsorption, cavitation, ion exchange, biological processes, oxidation, etc. [50]. In addition, shock treatment with sodium hypochlorite can inhibit the growth of biofouling in the dilute compartments of the RED unit. Injecting hypochlorite into the brine is unnecessary as the highly salty solution already inhibits the biofouling [51].

This study focuses on the feasibility of SGP production from a RED system that employs ammonia-rich industrial wastewater and high salinity brine as working fluids, with the proper use of the RED effluents as fertigation water in the subsequent FO process. This study will investigate the effect of HC and LC stream concentrations, compositions, and flowrates on the obtained power density and energy recovery in a lab-scale RED system. In addition, the effects of applied external loads, the number of membrane stacks, and recyclability of wastewater streams will be systematically analyzed and optimized to amplify the osmotically generated power and economically evaluate the RED-FO hybrid system.

2. Experimental

2.1. Chemicals and reagents

All chemicals used in this research were of analytical grade and used directly as received. Both model high and low-concentration solutions were prepared by dissolving ammonium sulfate ($(NH_4)_2SO_4$, Research-lab fine chem industries, 98.5 %) and sodium chloride (NaCl, Research-lab fine chem industries, 99.5 %) in deionized (DI) water. Potassium hexacyanoferrate (III) ($K_3[Fe(CN)_6]$, Sigma-Aldrich, 99.0 %), potassium hexacyanoferrate (II) trihydrate ($K_4[Fe(CN)_6]\cdot 3H_2O$, Sigma-Aldrich, 99.8 %) and NaCl were mixed and appropriately dissolved in DI water to form the recirculated electrolyte rinse solution.

2.2. Solution preparation

For the preparation of the HC streams, simulated brine ranges were prepared based on SWRO brine, assuming that SW was in the range of 3.5–4.2 wt% [3], and the RO recovery % was 35–50 % [52]. Accordantly, the HC stream concentrations varied from 0.75 M to 1.5 M of NaCl, corresponding to 45 mS/cm and 85.3 mS/cm, respectively. Regarding the preparation of LC streams, simulated ammonia-based WWs were prepared with concentrations of 0.005, 0.015, 0.03, and 0.06 M SOA to accommodate typical concentrations of WW streams produced from fertilizer-producing plants [49].

2.3. Reverse electrodialysis working principle

To understand the main working principle behind the controlled mixing of the respective high and low salinity solutions and, thereby, the resulting energy gain through the RED cell, it is necessary to look at how this membrane-based technology is constructed and built. Here, a typical RED stack consists of an array of alternatively arranged anion and cation exchange membranes (CEM and AEM), each separated by a flow-directing spacer, and the whole stack is sandwiched between two other cation exchange membranes with electrodes at the ends. This geometry of the membranes forms an array of concentration and dilution compartments. Fig. 3a illustrates the basic configuration of the RED cell with its working mechanism. From their names, the formed concentrating and diluting compartments are alternatively fed with the high and low salinity solutions, except for the terminal electrode compartments. These end electrode compartments or chambers are supplied with a solution containing a redox couple that is recirculated between the two end electrode compartments. Due to the semi-permeable characteristics of the anion and cation exchange membranes used, only anions (through AEM) or cations (through CEM) are ideally allowed to pass, the transport of co-ions and water is blocked, and only the respective counter-ions migrate from the concentrated to a dilute saline stream. This movement of ions towards the oppositely charged electrodes creates an ionic current in the stack, and an electric potential builds up on the membrane sides. The ionic current is then converted to an external output current (i.e., electron flux from the anode to the cathode) by a redox reaction at the electrodes.

2.4. RED experimental setup

A lab-scale commercial ED cell (PCCell GmbH, ED64002-020, Heusweiler Germany) was installed and adapted in a RED configuration to serve the intended RED application. Fig. 3b shows the commercial RED reactor and its components. The RED cell provides a flexible alteration of its ion exchange membranes that can reach up to 20 pairs of membrane cells (membrane size: 110 × 110 mm) stacked together, each holding a standard CEM (PC-SK), an AEM (PC-SA), and a woven-spacer. The cell offers a total membrane area of 0.13 m^2, with each membrane providing an active membrane area of 64 cm^2 (8 × 8 cm). The woven spacer between each membrane is 0.5 mm thick, which provides proper channel dimensional stability, and enhances the flow and mixing process. Tables 1 and 2 provide detailed specifications for the various membranes and the overall reactor specifications. The sides of the membrane stack are held by two-electrode compartments, each having a titanium mesh electrode coated with iridium and platinum (Pt/Ir-coated titanium). The electrode rinse solution was recirculated through the

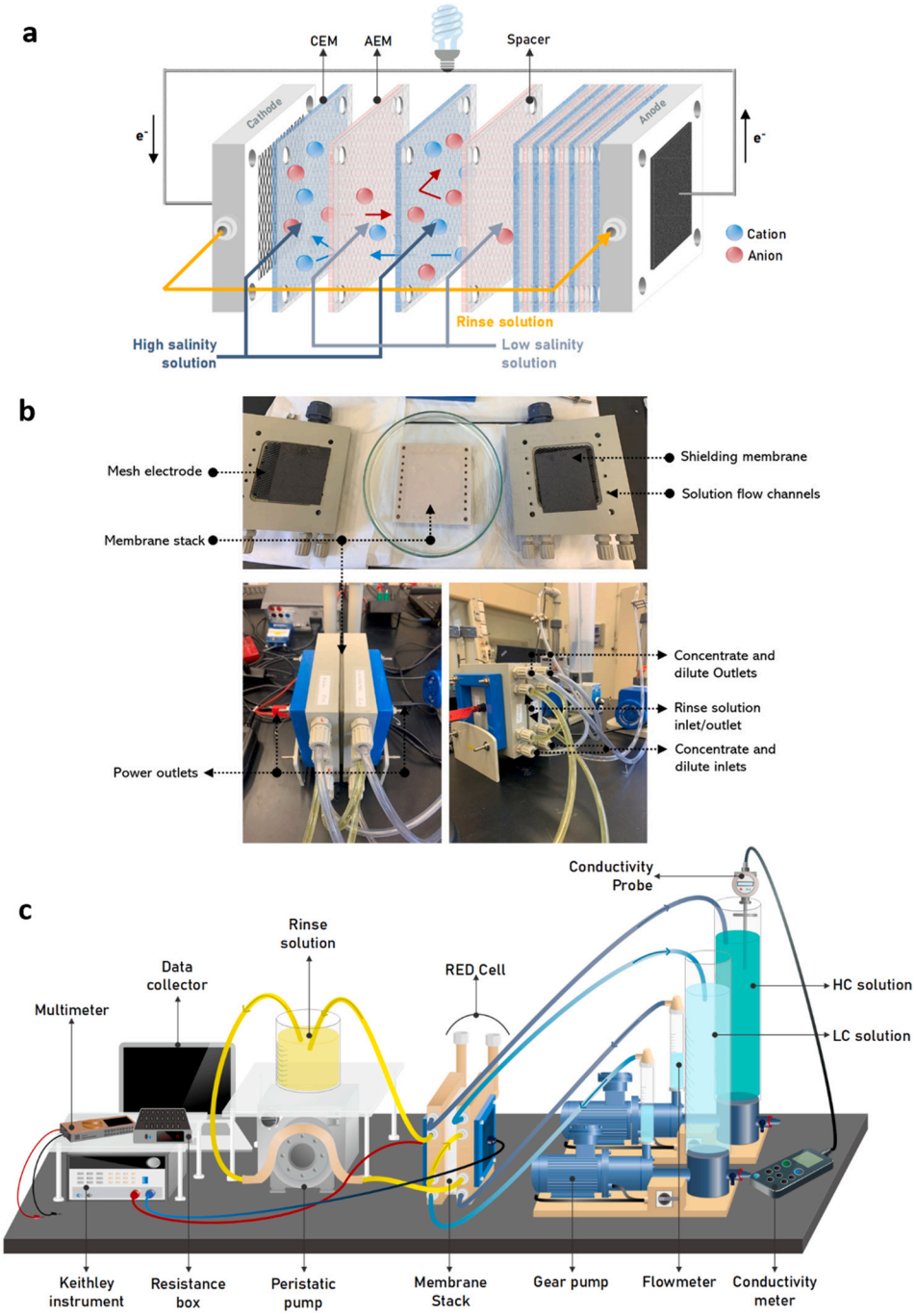

Fig. 3. (a) Principle of reverse electrodialysis (RED) with concentration profiles and ionic flux. (b) Bench-scale RED cell components and solution flow pathways. (c) Bench-scale RED setup used for experimental results retrieval.

corresponding electrode compartments in a closed-loop manner using a peristaltic pump (MasterFlex Cole-Parmer). Hexacyanoferrate (III)/hexacyanoferrate (II) (0.05 M $[Fe(CN)_6]^{2+/3+}$ in 0.5 M NaCl) redox couple was used as the electrode rinse solution due to its low toxicity and high level of stability [37]. Each HC and LC solution stream was passed through a separate 2 L vessel connected to a gear pump and a flow meter, after which it was channeled through the pumps and flow meters to the RED cell inlets (Fig. 3c). Two proton exchange membranes (PEMs) (Nafion membranes) were used at both ends of the membranes stack and in contact with the anode and cathode compartments to prevent the undesirable mixing of the feed and rinse solutions.

2.5. RED tests and evaluation methods

In each RED test, the system was initially stabilized by flowing DI water for 10 min through both HC and LC solution compartments to ensure proper wetting of all membranes and flow channels. Next, a second stabilization step was performed by allowing the HC and LC solutions to flow through the process channels for an additional 10 min. During the runs, the HC and LC solution's conductivity measurements were taken regularly using a conductivity meter (HQ14D, Hach). As shown in Fig. 3c, the two ends of the RED cell were connected to a variable external load (resistance box, Sfernice) whose external resistance varies between 5 Ω and 100 Ω. An external circuit was also connected to a multimeter (Fluke) in series with the RED cell and the

Table 1
Properties of the ion-exchange membranes used in the present study.

Membrane	AEM	CEM	End membrane
Thickness (μm)	100–110	100–120	220
Ion exchange capacity (meq/g)	1.2	3	1.8
Resistance (Ω cm^2)	~1.8	~2.5	~4.5
Burst strength (kg cm^2)	4–5	4–5	15
Water content (wt %)	~14	~9	–
pH stability	0–9	0–11	1–13
Maximum temperature (°C)	60	50	40
Membrane type	Strongly alkaline (ammonium)	Strongly acidic (sulfonic acid)	Strongly acidic (sulfonic acid)
Reinforcement	Polyester	Polyester	Polyethylene

Table 2
General properties and specifications of the RED stack used in the analysis.

Specification		Value
Effective membrane area (cm^2)		64
Membrane size (cm)		11 × 11
Spacer thickness (mm)		0.45
Processing length (mm)		80
Compartment width (mm)		165
Effective membrane area/unit (max m^2)		0.38
Membrane spacing	Electrode-membrane (mm)	Ca. 1
	Overcell (mm)	0.5
Spacer	Thickness (μm)	450
	Mesh orientation to flow direction	45°
	Porosity	82.5 %
	Material	Silicon/polypropylene
Cell frame and tube material		Polypropylene
Pressure drop over cell		Max, 0.5 bar

resistance box to measure the output current (mA) and the potential drop across the external load. In each experiment, the output current and voltage were measured using a source meter unit (Keithley 2400 Standard Series SMU) at 30-minute intervals for 2 h. In addition, the open-circuit voltage was measured through a potentiostat (Gamry, Interface 1010E Potentiostat) for 200 s. A linear current sweep from 0 to 0.3 A was applied with a 5 mA step size using Keithley KickStart software (Tektronix, Oregon, USA) for the output voltage and associated current measurements.

In the experimental runs, variables such as solution composition, concentration, flowrates, process flow mode, external load added, and the number of membrane stacks were changed depending on the type of effect to be studied. In contrast, others, such as the composition and flowrate of the rinse solution, were fixed. Table 3 provides experimental details for both constant and variable parameters applied in this study.

In all RED studies, the main parameter used to evaluate the RED stack performance is the power density (P_d) of the stack, sometimes referred to as gross power density (P_{gross}, W/m^2), as it provides a comprehensive measure of the electrical energy generated per cell-pair area:

$$P_{gross} = \frac{P}{N \cdot A_m} \tag{1}$$

where N is the number of cell pairs and A_m is the effective area associated with a single cell membrane pair. Here, P (W) is the power output from the cell and is given by:

$$P = E_{Stack} \cdot I_m \tag{2}$$

To evaluate the stack voltage (E_{Stack}), the voltage produced due to the presence of the external load must be taken into consideration and subtracted from the measured output voltage (E_m) using the following relationship:

$$E_{Stack} = |E_m - I_m \cdot R_u| \tag{3}$$

where I_m is the measured output current (obtained directly from Keithley device) and R_u is the resistance of the external load in Ω. Theoretically, the output voltage ($\boldsymbol{E}$) of the stack should be the total sum of the cell voltages minus the effect associated with the total internal resistance of the system (R_{stack}, $\Omega \cdot m^2$) [11], according to the relationship:

$$E = \sum E_{cell} - jR_{stack} \tag{4}$$

where j stands for the current density (A/m^2). Nevertheless, this theoretical equation can be modified by using the measured OCV values with I_m to facilitate practical use, giving the following relation:

$$E_{Stack} = OCV - R_{Stack} I_m \tag{5}$$

Rearranging Eq. (5) [51] gives a reasonable estimate of the amount of R_{stack} by:

$$R_{Stack} = \frac{OCV - E_{Stack}}{I_m} \tag{6}$$

To obtain a more reasonable and practical estimate of the RED performance, the P_{gross} value is usually modified by subtracting the power consumed in pumping the working fluids normalized to the total cell-

Table 3
Experimental details applied in this study.

Experimental details	Composition and concentration		Initial flow velocity	External load added	Number of membrane pairs	Flow mode	Experiment duration	Rinse solution
	HC solution	LC solution						
Solute composition effect	1 M NaCl 1 M SOA 1 M SOA-NaCl	0.015 M NaCl 0.015 M SOA 0.015 M SOA-NaCl	0.64 cm/s	5 Ω	10 membrane pairs	Recirculation mode	2 h	Composition: 0.05 M $[Fe(CN)_6]^{2+/3+}$ in 0.5 M NaCl Conductivity: 43.9 mS/cm Flow velocity: 0.64 cm/s
Solute concentration effect	0.75–1.5 M NaCl	0.005–0.06 M SOA						
Flow mode effect	1 M NaCl	0.015 M SOA				Recirculation mode/ single pass mode		
Flow velocity effect			0.25–3.55 cm/s			Recirculation mode		
External load effect		0.015 M SOA 0.03 M SOA 0.06 M SOA	0.64 cm/s	0 Ω, 5 Ω, 10 Ω, 50 Ω, 100 Ω.				
No. of membrane pairs effect		0.015 M SOA		5 Ω	10 to 20 membrane pairs			

pair area of the stack. This gives the net power density of the stack (P_{net}) according to:

$$P_{net} = P_{gross} - \frac{P_{pump}}{N \cdot A_m} \tag{7}$$

$$P_{pump} = \frac{\Delta P_{HC} \cdot Q_{HC} + \Delta P_{LC} \cdot Q_{LC}}{\eta} \tag{8}$$

where ΔP_{HC} and ΔP_{LC} refer to the pressure drops (P_a) between the inlet and outlet compartments of the high and low concentration solutions, respectively, in a spacer-filled system. On the other hand, Q_{HC} and Q_{LC} here represent the respective HC and LC solutions volumetric flowrates (m^3/s), while η is the efficiency of the pump which was set to 75 % as considered elsewhere [51,53].

In this study, the working fluid flowrate is analyzed by converting it to the average fluid flow velocity (v) estimated in a single spacer-filled channel using:

$$v = \frac{Q}{\delta \cdot b \cdot \varepsilon_{sp}} \tag{9}$$

where v is measured in m/s, Q is the volumetric flowrate (m^3/s) of the desired solution (LC, HC or rinse solution), δ is the thickness of the spacer, b is the width of the compartment, and ε_{sp} is the porosity of the spacer. The values of all these denominator constants are provided in Table 3.

Next, an important parameter in the RED performance analysis is the overall resistance of the system, which has a proven effect on most of the performance parameters and is a major factor in reducing the power density obtained from the RED system. The total resistance usually consists of the external load resistance (R_u) and the internal resistance of the stack (R_{Stack}). Eq. (6) provides a numerical estimate of the R_{Stack} value. However, it is significant to understand the implication behind it. The value of R_{Stack} is influenced by some significant ohmic and non-ohmic contributions. The ohmic contributions include the membrane resistance of the cation and anion exchange membranes (R_{CEM} and R_{AEM}), as well as the low and high concentration compartment resistances ($R_{LC}$and R_{HC}). In some cases, the electrode compartment resistance is added, but this effect is mostly negligible for cells with a large number of stacks [12]. On the other hand, the non-ohmic contributions to the internal resistance of the stack include the resistance caused by the change in the stream concentration along with the compartments (R_{AC}) and the resistance due to the creation of diffusion boundary layers (DBLs) inside the dilutive and concentrative compartments.

$$R_{Total} = R_u + R_{Stack} \tag{10}$$

$$R_{Stack} = R_{Ohmic} + R_{non-Ohmic} \tag{11}$$

$$R_{Ohmic} = R_{CEM} + R_{AEM} + R_{HC} + R_{LC} + R_{el} \tag{12}$$

$$R_{non-Ohmic} = R_{AC} + R_{DBL} \tag{13}$$

Finally, the yields of the gross and net power densities were estimated as the amount of power generated per cubic meter of the flowing LC solution:

$$Y_{gross} = \frac{P_{gross}}{Q_{Low}^{Tot}} \tag{14}$$

$$Y_{net} = \frac{P_{gross}}{Q_{Low}^{Tot}} \tag{15}$$

2.6. Forward osmosis (FO) experiments

The experimental bench-scale FO setup consists of feed solution (FS) and draw solution (DS) tanks, two variable gear pumps (Cole-Parmer, USA), two flowmeters (Cole-Parmer, USA), PVC tube fittings, 3/8″ steel tube fittings, and a handmade FO test cell. In addition, a commercial flat-sheet thin-film composite (TFC) (Toray Industries, Inc. (Toray)) was put into the FO test cell. For immediate weight changes of the DS, the DS tank was placed on a digital scale connected to a PC. In addition, the water circulates from the feed side to the draw side in a closed loop since the FO test cell has two symmetric channels on either side of the membrane. For the hybrid RED-FO system, all FO experiments were operated in FO mode with the active layer of the FO membrane facing the FS side. Initially, DI water was used as FS and DS for 30 min to stabilize the FO process. Then, FO tests were performed for 5 h at various DS concentrations, outlet of RED, fixed flowrates (1 L/min) of bulk solution, FS concentration (0.1 M) and room temperature (25 °C ± 2). To reduce membrane fouling, in-situ hydraulic flushing was applied for 30 min after each FO test using DI water as FS and DS. The performance of the FDFO process was evaluated in terms of water recovery % and average water flux (J_w) as expressed in Eq. (16), where ΔW is the weight changes of DS, Δt is the operating time, and A_{eff} is membrane-effective area. Also, the FS and DS water quality was recorded before and after each FO test using (HQ1400 portable multimeter, HACH, USA).

$$J_w\left(L \cdot m^{-2} \cdot h^{-1}\right) = \frac{\Delta W}{\rho\, A_{eff}\, \Delta t} \tag{16}$$

3. Results and discussion

3.1. Influence of HC and LC solution concentration and composition

To properly optimize the performance of the RED unit for its intended application, a comparative analysis was first implemented with feed solution components. Here, the functionality of several single-component systems was evaluated and compared with multi-component systems to simulate and reflect the use of different industrial feed stream pairs in the RED system. The HC and LC compartments in each single-component system were fed with solutions containing the exact type of dissolved solutes. For this analysis, the LC solution concentration was set to 0.015 M, while the concentration of the HC solution was chosen to be 1 M. Both LC and HC compartments were fed with an initial constant flowrate of 20 mL/min, corresponding to a linear velocity of 0.64 cm/s. All systems were examined with the same operating parameters of a 5 Ω external load, 10 membrane cell pairs, and two hours of operation at 24 °C. The results for the NaCl, ammonium sulfate (SOA), NaCl/SOA single component systems, and the NaCl and SOA multi-component systems are shown in Fig. 4. These systems were investigated for their initial and final HC solution salinities, their maximum gross power densities ($P_{d,max}$), and their maximum open-circuit voltage (OCV_{max}) obtained in each run. Overall, the NaCl single-component system reached approximately 2.57 W/m^2, achieving the highest power density, followed by the NaCl/SOA single-component system and then the SOA single-component system at $P_{d,\,max}$ of 1.47 W/m^2 and 0.99 W/m^2, respectively. However, this tendency to gain power between the single-component systems does not necessarily reflect the difference in salinity between the two feed compartments. For instance, the high power density generated in the NaCl single-component system is accommodated with a salinity gradient of around 58.5 mS/cm between the 1 M HC (EC = 60.9 mS/cm) and 0.015 M LC (EC = 1.35 mS/cm) feed solutions, respectively. On the other hand, the SOA single-component system has a 36.7 % higher HC solution conductivity (SOA HC solution = 94.9 mS/cm) than the former NaCl solution system (Fig. 4), and the salinity difference between the feed solutions reached around 92.5 mS/cm. Nevertheless, this high salinity difference, the main electromotive driving force of the RED process [54], was not reflected in the energy generated (0.996 W/m^2), thus, highlighting the importance of the composition of the feed for the system performance. In these circumstances, using high salinity SWRO brine in the HC compartment shows prominent advantages in energy harvesting with lower salinity

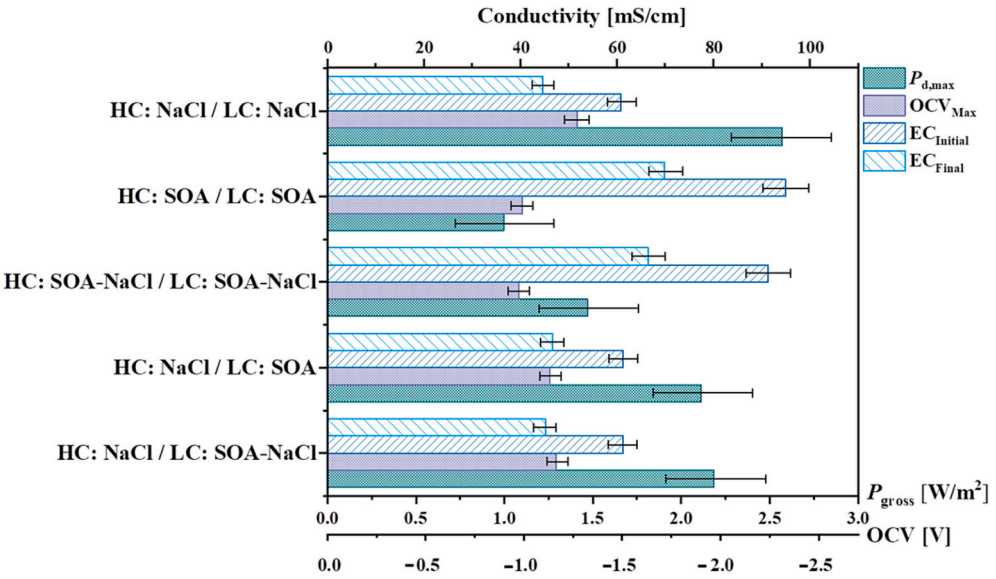

Fig. 4. Primary power generation and feed composition analysis for single and multi-component systems. Evaluation was conducted at constant initial concentrations (0.015 M/1 M) of LC and HC solutions, a linear flow velocity of 0.64 cm/s, 10 Ω external load, and 10 cell membrane pairs.

gradient requirements than the investigated alternative SOA and NaCl/SOA HC solutions. The incorporation of SOA in the LC feed solution, forming multi-component systems, reduced the overall $P_{d,\ max}$ of the RED unit when fixing NaCl as the HC solution. When the RED system using pure NaCl as LC was replaced with NaCl/SOA and pure SOA, the $P_{d,\ max}$ values were reduced by 14.89 % and 17.79 %, respectively. Although the inclusion of SOA reduces the power density to some extent, the potential of SGP generation can be fully exploited by applying ammonia-based wastewater and brine as RED feed solutions.

The basis of power generation of the RED system is the conversion of the ionic charges into electrical currents. This ionic current is the virtue by which an internal potential difference is established in the RED stack due to the flow of the HC and LC streams across each other [12]. Thus, a determining factor for power gain in this process is the appropriate assessment of the HC and LC solution salinities and established gradients, along with the analysis of any limitations associated with this property. Here, several tests on the lab-scale RED setup were conducted to evaluate the potential of SWRO brine and ammonia-based WW as HC/LC couple for power generation.

The tests were performed with a stack of 10-membrane pairs at a fixed initial linear flow velocity of 0.64 cm/s for both the HC and LC solutions and a fixed flow velocity of 0.64 cm/s for the redox couple ($[Fe(CN)_6]^{2+/3+}$) flowing through the electrode chambers. In these trials, an external load of 5 Ω was applied, and the feed streams were recirculated for two hours. First, the effect of the LC solution concentration on RED performance was investigated using LC solution concentrations ranging from 0.005 M to 0.06 M SOA while maintaining 1 M NaCl HC solution for all runs. The reason for using these LC concentrations is that WW effluents from fertilizers-producing plants have ammonia nitrogen contents ranging from 7 to 1700 ppm [49], corresponding to approximately 0.035 mM to 0.09 M SOA. Therefore, simulated ammonia-based WW with 0.005, 0.015, 0.03, and 0.06 M SOA concentrations were

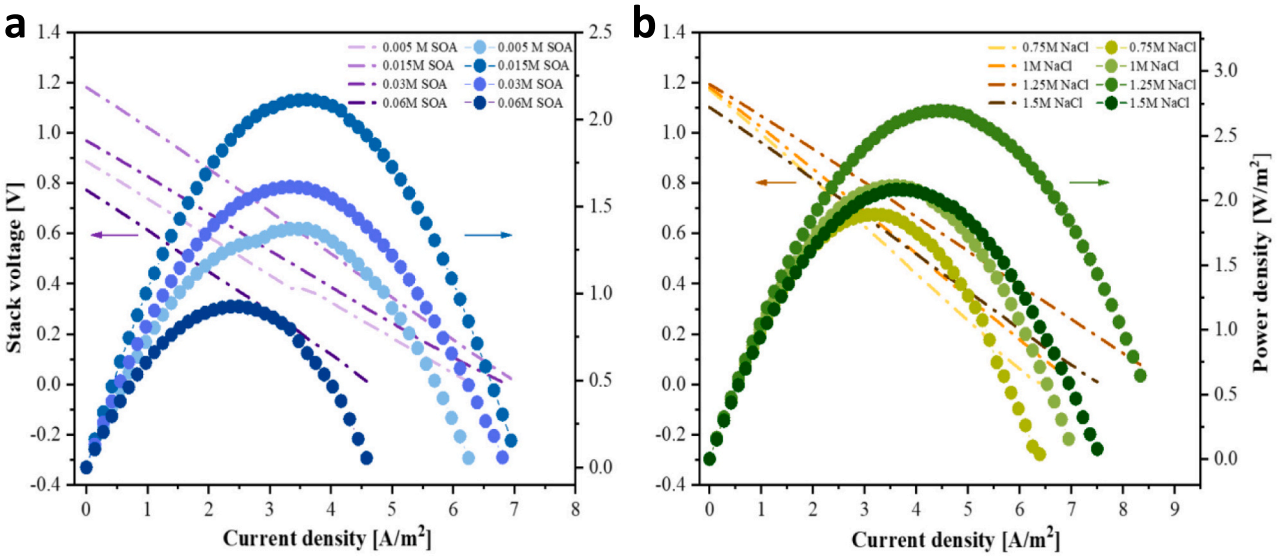

Fig. 5. RED process performance is influenced by; (a) Various dilute solution concentrations (LC) ranging from 0.005 M to 0.06 M SOA at fixed HC of 1 M NaCl. (b) Various high solution concentrations (HC) ranging from 0.75 M to 1.5 M SOA at a fixed LC of 0.015 M SOA. The RED process was operated at a constant flow rate of 20 mL/min, applied resistance of 10 Ω, with 10 membrane cell pairs.

selected to accommodate most of this concentration range.

Fig. 5a shows the trends of power density ($P_{d,\ max}$) and stack voltage (V_{stack}) as a function of applied current densities ranging from 0 to 0.3 A for various LC concentrations. When the LC SOA concentration is lowered from 0.06 M to 0.015 M, $P_{d,\ max}$, and associated stack voltage trends increase by 40 % from 0.924 W/m^2 to 2.1 W/m^2 due to the increase in electromotive driving force. This consistent increase in power density can be attributed to the rise in salinity ratio (energy input) between the HC and LC solution compartments. According to Zhu's study [13], the LC concentration is a significant contributor to the total internal resistance of the stack, where performance loss arises along with a decrease in the LC concentration due to an increase in the ohmic solution resistance. However, for SOA LC concentrations >0.015 M, the effect of solution resistance on power density appears to be less significant because of the trade-off between the high increase in salinity gradient difference and the steady internal resistance growth. On the other hand, when LC salinities drop below 0.015 M, the internal resistance growth plays a considerable role in reducing the performance and power density. As shown in Fig. 5a, reducing the LC concentration to 0.005 M causes the $P_{d,\ max}$ to decrease to 1.6 W/m^2 at an applied current density of 3.33 A/m^2. These trends are consistent with similar NaCl LC concentration plots presented elsewhere [11,55,56].

The power generation of the RED system by HC concentration with high conductivity was strongly influenced by the permselectivity of anion and cation exchange membranes. Fig. 5b demonstrates this effect by varying the HC concentrations between 0.75 M (EC = 44.1 mS/cm) and 1.5 M (EC = 85.3 mS/cm) NaCl, at constant LC solution of 0.015 M SOA. The maximum power density constantly increased from 1.89 W/m^2 in 0.75 M NaCl to 2.69 W/m^2 in 1.25 M NaCl, and then a further increase in HC concentration to 1.5 M causes the $P_{d,\ max}$ to drop back to 2.09 W/m^2. The initial surge of power generation when the HC concentration was increased up to 1.25 M NaCl is due to an increase in the salinity ratio, leading to an increase in the ionic current. Furthermore, the combined consequences of higher HC concentrations and increased salt crossover from the HC to the LC channels reduce the ohmic solution and non-ohmic diffusion boundary resistances, improving the power generation efficiency [11]. After that, the observed decline in performance at elevated simulated brine concentrations (HC > 1.25 M) can be ascribed to the decreased ion transport capability of the IEM due to the suppression in the Donnan exclusion capacity of the membranes with very high solution concentrations. The results show that the proper selection of feed solution couple's concentration with SWRO brine and

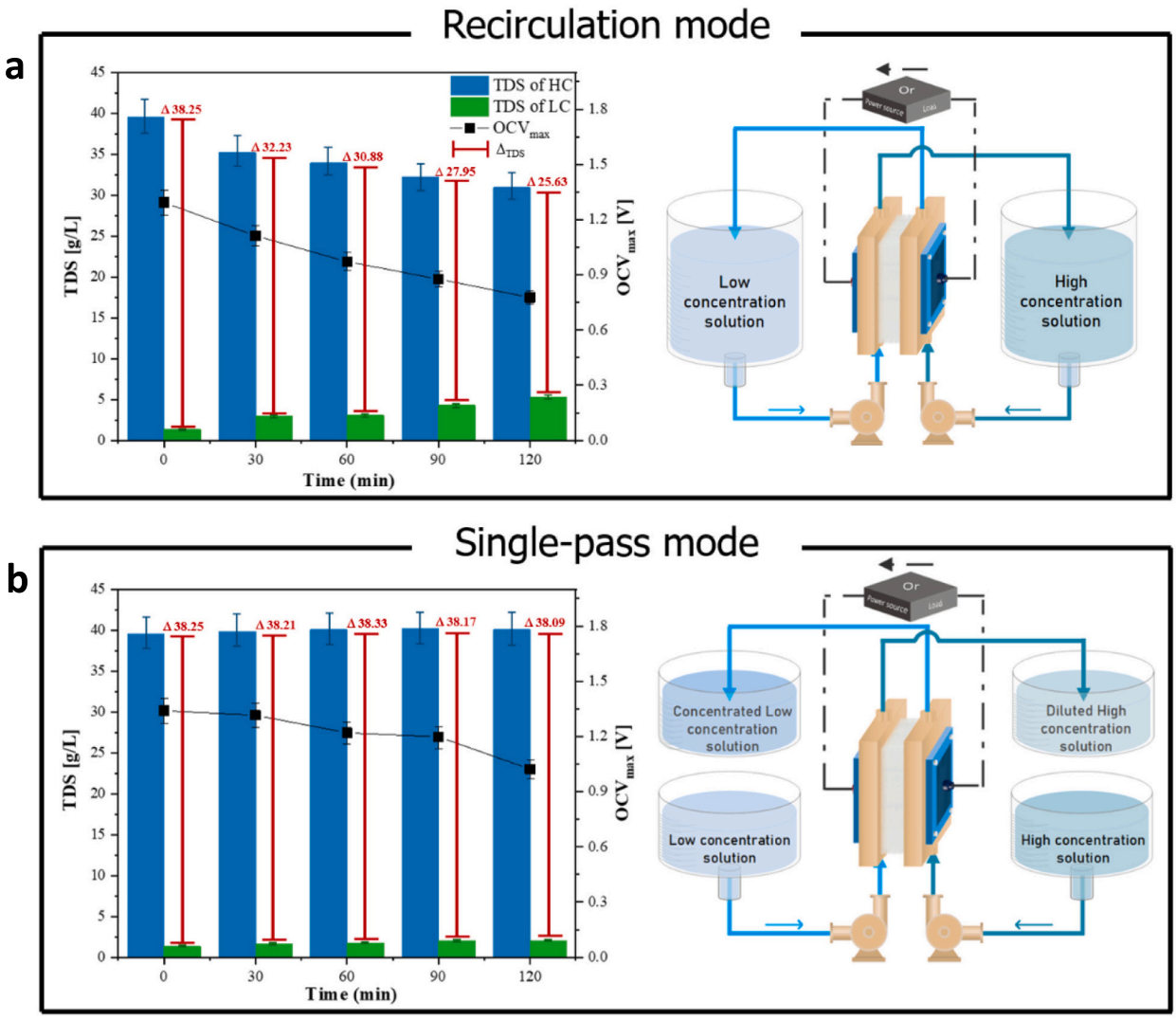

Fig. 6. Schematic diagram for the flow geometry of feed water applied to RED: (a) Recirculation mode. (b) Single-pass mode. For both operation modes, the RED process was performed for 2 h using a 0.015 M SOA/1 M NaCl LC/HC solution combination at a constant flow rate of 20 mL/min, applied resistance of 10 Ω, with 10 membrane cell pairs.

ammonia-based WW is crucial for the performance of the RED system. Having the lowest concentration of LC with the highest concentration of HC does not always give the highest power generation performance; there must be a sufficient number of ions that can pass through the RED cell membranes and form an ionic current with proper suppression of associated internal resistances initiated inside the membrane stack. Henceforth, 0.015 M SOA with 1 M NaCl LC and HC solution concentrations were chosen as optimal and representative concentrations for the following variable effects presented in this study.

3.2. Influence of solution flow mode and operation period

The effect of salinity gradient on RED performance was further validated by studying the impact of the RED operation duration and circulation mode. Fig. 6 presents the readings of maximum open-circuit voltages (OCV_{max}), and the correlated salinity gradient ranges expressed as the total dissolved solids (TDS) present in both feeds attained at 30-minute increments after the start of the experiment. Fig. 6a demonstrates the use of the HC and LC solutions in the RED system with a recirculation mode. In this mode of operation, the HC and LC solutions effluents are returned to the feed tanks of HC and LC solutions, respectively. As the run proceeds with time, the concentration of the HC solution gradually decreases from 39.59 g/L to 30.93 g/L, while the concentration of the LC solution increases from 1.34 g/L to 5.31 g/L. This steady change in solution dynamics is due to the gradual mixing of the HC and LC solutions as they pass against each other through the membrane stack. After mixing, the high and low-concentration solutions are returned to the influent reservoirs, diluting the HC solution and concentrating the LC solution simultaneously.

As a result, continuous circulation of these feed solutions for 2 h lowered the concentration gradient between the LC and HC solutions over time, reducing the salinity gradient by 33 % from 38.3 g/L to 25.6 g/L. As shown in Fig. 6a, this constant decrease in salinity gradient is directly proportional to the maximum OCV attained at that specific time. A lower salinity gradient between the flowing HC and LC solutions means a reduction in the electromotive driving force for power generation in the RED system (as described in Section 3.1 above). Therefore, the OCV_{max} is seen to experience a steady decrease with the operation time from 1.3 V at time 0 to 0.78 V after 2 h of a continuous operation as the concentration gradient gradually decreases. Consequently, the best performance was achieved at the beginning of the run with the highest salinity gradient.

One way to improve the amount of energy gained and preserve it for a longer duration is to change the circulation mode of the solutions by allowing the HC and LC solutions to pass through the RED cell only once and having two outlet reservoirs to avoid the mixing of those solutions outside the boundaries of the RED membrane stacks. Fig. 6b illustrates this attempt by switching to a single-pass mode. The extent of the electromotive driving force was maintained throughout the run, and the salinity gradient was held at 38 ± 0.24 g/L, reflecting a generally steady power generation (less negative slope) with an average power density of about 2.1 W/m^2. Nevertheless, there is still an observed decrease in the OCV_{max} values as time passes (from 1.34 V at time 0 min to 1.02 V at time 120 min) due to the restriction of the more dominant influence of solutions being mixed in the single-pass mode. Such behavior can be attributed to the gradual salt buildup at the surface of the CEMs and AEMs, which limits ion transfer across the membranes and subsequently weakens the ionic current as a function of time.

From a practical perspective, when these feed flow modes are applied in the SWRO plant with high volumes of feed solutions, a trade-off would be initiated between the energy obtained from a single RED run and the volume of saline streams consumed to generate this power. For instance, the energy-to-volume ratios obtained from the small RED stack used in this study were 0.77:1 (W/m^2·h: L/h) and 0.41:1 (W/m^2·h: L/h) for the recirculation mode and single-pass mode, respectively. With these effects, a simple and effective strategy for optimizing energy performance and maintaining a high power yield-to-volume ratio is to flow the feed solutions through multiple independent RED cells placed in series to keep high energy generation with low feed volumes. This is because feed dilution is minimized. The RED in series systems has shown strong effectiveness in several theoretical [15] and experimental studies [16,57,58]. For instance, Veerman et al. [58] demonstrated an experimental attempt to assess the use of a four-stage 50-cell pair RED system in series. In their study, the peak net output power and cumulative energy efficiency reached 0.96 W and 18 % when three RED stages were employed in series. Also, a recent study [16] shows that the output power and unit work potential were improved from 0.28 W and 0.45 kJ kg^{-1} for a single RED system to 0.92 W and 1.63 kJ kg^{-1} for 8 RED stages in series. Both cases have the same number of ion-exchange membranes. The main reason behind this enhancement is attributed to the fact that having multiple RED stages in series allows for the proper adjustment of the output voltage according to the variation in the concentration difference between HC and LC solutions. Thus, the multiple RED stages in series can avoid the creation of the electrodialysis phenomenon that occurs when using a single stage RED system with a large number of cell pairs leading to the drainage of the generated power, thereby enhancing the captured salinity gradient energy.

3.3. Influence of solution velocities

The effect of flow velocity on RED performance was investigated using the optimal LC, and HC concentration mixture previously established with 0.015 M SOA/1 M NaCl. Using Eq. (9), estimates of the mean fluid flow velocity inside a single spacer-filled channel were obtained. The parametric analysis was performed at a flow velocity of 0.25–4 cm/s for both dilute and concentrate streams with 10 IEM pairs at 24 °C. To properly evaluate the extent of energy acquisition more practically, net power densities were obtained by considering the power consumed in pumping the fluids (considering the pressure drops along with the compartments) and deducting it from the gross power density.

Fig. 7a shows the effect of the feed flow velocity on the RED performance concerning the maximum gross power density (P_{gross}), net power density (P_{net}), and obtained OCV. As a result, the gross and net power densities increase to 2.17 W/m^2 and 2.14 W/m^2 as the feed velocity increases only to 1.18 cm/s. Then, the power values obtained at higher flow velocities experience a steep decline with some divergence between the $P_{gross,\ max}$ and the $P_{net,\ max}$. The initial growth in power gain is due to a reduction in the residence time of the flowing solutions, which leverages an increase in the salinity gradient between the HC and LC compartments and improves their mixing, thereby increasing the driving force for the controlled ion transport across the membranes. Also, developing a uniform concentration gradient between the solution compartments reduces the values of internal resistance components, R_{AC} and R_{DBL}, so R_{stack} appears to decrease significantly with higher flow velocities (Fig. 7b). In turn, the lower internal resistances experienced provide an opportunity for higher energy gain.

Given the pressure drop along the compartments and the gradual linear increase and dominance of the P_{pump} as the flow velocities surges above 1.18 cm/s (Fig. 7a), the acquired power densities and OCV become progressively lower as hydraulic losses become more significant, causing the P_{pump} to reach 5.80 W at ~4 cm/s. A similar trend of a decrease in performance after reaching a particular flow velocity value was reported in a study by Tedesco [59], where net power density decreased at flow velocities above 1 cm/s. The main reason for this decline is that in regions with high flow velocities, the residence time of the solutions in the compartments is considerably shortened, deriving the outlets of the solutions away from the equilibrium. As a result, only a tiny portion of the achievable potential energy is recovered. Fig. 7b shows the resulting gross and net yields transferred by the amount of energy produced per cubic meter of the feed solution. Both values continue to decline with increasing flow velocities, even below 1.8 cm/s. This declining trend was found and explained in Hu's work [16], where

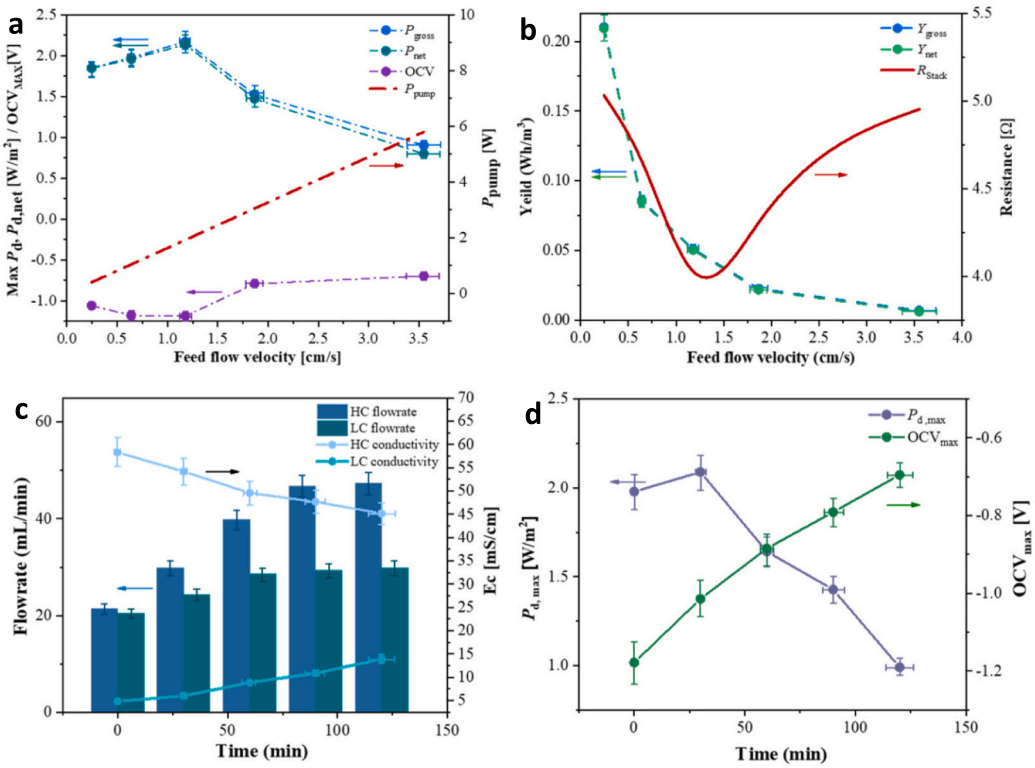

Fig. 7. Effect of feed flow velocity on RED process performance. (a) Gross and net power density, pumping power, and OCV. (b) Internal resistance and (gross and net) yields. Experimental progress effects on (c) flowrate and (d) maximum power density and OCV. The RED process was run using the recirculation mode at 0.015 M SOA/1 M NaCl solution and 10 Ω external load with 10 membrane cell pairs.

the reduction pattern was attributed to the enforced passage of co-ions through the membranes as the velocities of the solutions get higher, causing a deceptive mixing of the saline solutions without contributing to the power generation of the RED stack.

Next, further analysis regarding the effect of HC and LC flow velocities on power generation was performed with the RED in the recirculation operation mode. Fig. 7c and d demonstrate this effect by displaying the flowrates and conductivities of the feed solutions along with the maximum gross P_d and OCV attained over various run periods. As the run time progressed, the HC and LC flowrates gradually increased while their respective salinities got close. These two effects do not compete with one another but amplify each other, lowering the overall power densities and OCVs. Notably, as the salinity gradient between solutions decreases, the mixing phenomena is propagated by solution recirculation (as discussed in the previous section of this study), and the solutions rapidly reach equilibrium, increasing the fluid flow velocities of the two solutions inside the cell compartments. Here, the feed flowrates start their increase with increments of 28.1 % and 15.9 % per 30 min and end with a rise of 15.9 %/30 min and 1.77 %/30 min for HC and LC solutions, respectively. On the other hand, as previously discussed, the progressive increase in flowrates above 40 mL/min (1.18 cm/s) substantially reduce the residence time of the solutions, thereby reducing energy attainment. In this case, choosing flow velocities in the range of 0.5 cm/s to 1.5 cm/s provides an appropriate balance between the obtained power densities and fluids pumping power consumption in the RED system.

3.4. Best performance parameters including influences of applied external load and number of membrane cell pairs on RED energy acquisition

As described previously, the effect of feed solution concentrations on RED performance is highly influenced by the amount of internal resistance provided by the solutions flowing across the internal RED stack compartments. Another factor that can alter the overall system performance is the relative contributions between the individual resistive components that affect the total resistance of the system. The overall resistance of the RED system consists mainly of the internal resistance of the stack and the resistance added by the external load applied, as described in Eq. (10). Fig. 8 presents the results for the performance of the RED unit under various applied external loads of 5 Ω, 10 Ω, 50 Ω, and 100 Ω at LC concentrations of 0.015 M, 0.03 M, and 0.06 M SOA. The general trend of the data follows a decreasing pattern as the readings move from 0.015 M to 0.06 M SOA solutions, similar to the pattern shown in Fig. 5a. However, the response of the power density data to various applied resistances was distinct for each LC concentration scenario. Here, in all scenarios and regardless of the amount of external load applied, the power density readings fall within the same range at low current densities (lower than 2.77 A/m^2) and deviate from those values at higher ones. In Fig. 8a, the application of 50 Ω and 100 Ω provides lower maximum peaks than the case of applying 5 Ω and 10 Ω, which gives the best performance out of all (2.32 W/m^2 at 10 Ω external load). Next, in Fig. 8b, 5 Ω has the best performance, 10 Ω is lower than that, and 50 Ω and 100 Ω show intermediate values between the 5 and 10 Ω results. Readings at 0.06 M SOA (Fig. 8c) show a reverse pattern in the assortment of its $P_{d,\ max}$ values compared to Fig. 8a under various applied loads.

A closer look at the effects of internal resistance is needed to understand these distinct patterns. Fig. 9 shows the relative contribution of the added load resistance (R_u) to the measured current (I_m), voltage (E_{stack}), and OCV. It also demonstrates how these values affect the internal resistance of the stack and, thereby, the obtained maximum power densities for the three scenarios explored. As described above, high values of OCV and $P_{d,\ max}$ at low LC solutions are caused by the decreased resistances in the solution compartments, which leads to an

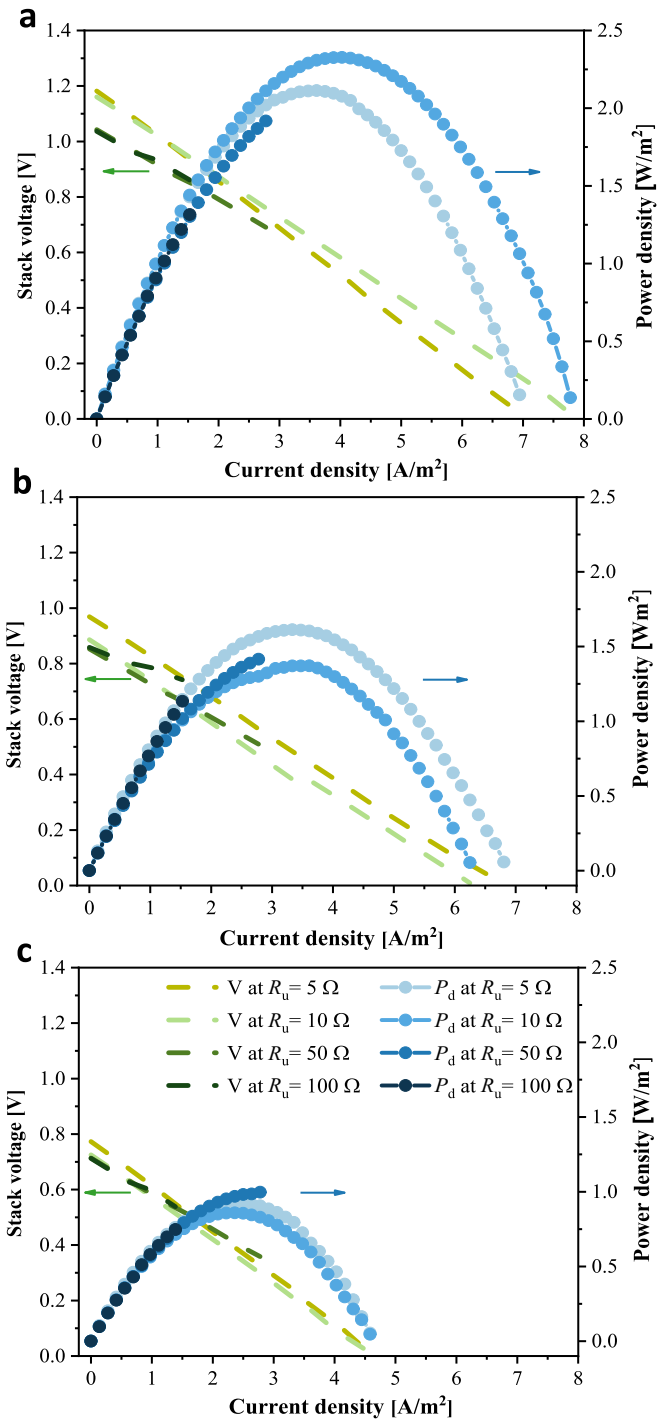

Fig. 8. Evaluation of gross power density and stack voltages for the RED process at various external loads using different LC solution combinations of (a) 0.015 M SOA, (b) 0.03 M SOA, and (c) 0.06 M SOA with HC solution of 1 M NaCl. Results were obtained by recirculating the feed solutions at 20 mL/min, using 10 membrane cell pairs and 10 Ω of external load.

overall reduction in R_{stack} and a corresponding increase in $P_{d,\ max}$ (Fig. 9a). For all LC concentrations, an increase in the external load value usually causes an increase in the measured E_{stack} values at $P_{d,\ max}$. Going from 0 Ω to 100 Ω applied external load, an average increase of 27.7 % in the measured E_{stack} values is observed. Despite this, the maximum OCV values remained constant at 1.293 V, 1.084 V, and 0.884 V with increasing R_u. As shown in Fig. 9, there is a distinct inverse relationship between the highest power density acquired in each run and the developed stack resistance. Here, as the external load varies, the lowest R_{stack} values for each LC solution are always associated with the highest $P_{d,\ max}$ in the run. Specifically, in the case of 0.015 M LC solution, the highest $P_{d,\ max}$ (2.2 W/m^2) occurred when an external load of 15 Ω was applied, because the measured highest current (I_m = 0.145 A) resulted in the lowest R_{stack} development (4.94 Ω). A similar pattern can be observed for the other cases where the highest $P_{d,\ max}$ (1.6 and 0.99 W/m^2) are correlated with the measured lowest currents of 0.13 A at 5 Ω and 0.1 A at 50 Ω, giving the lowest R_{stack} values of 4.92 Ω and 5.25 Ω for 0.03 M SOA and 0.06 M SOA, respectively. As a result, the power obtained from the RED stack depends on the potential difference between the electrodes (OCV and E_{stack}), the internal resistance of the stack, and the external load resistance [12]. At this point, choosing 10 Ω as the best-performing unit for this parameter is quite considerable, as it shows the maximum and most consistent power generation in most studied scenarios.

According to the results above, the internal resistance developed inside the RED stack is a single common major factor that can affect the overall performance of the RED process. Here, developing high values of R_{stack} reduces the acquired power densities, thereby decreasing the process performance. Fig. 10a illustrates the contributing factors to the growth of R_{stack} inside the RED cell. The value of R_{stack} can be reduced through the precise control and increase of the HC-LC concentration gradient, either by changing the composition and concentration of the flowing solutions or by changing the flow mode of the system. Furthermore, by monitoring the solutions' flow velocities (increasing to a specific limit) and the amount of external load added, the extent of internal resistance can be controlled to provide the best RED performance.

To further maximize the RED performance, an important constraint that can significantly affect the energy production and limit the scalability and associated costs of the RED process is the number of membrane cell pairs (membrane stacks) applied to the system. Fig. 10b shows the OCV and maximum power densities achieved with the RED stack at maximum power-generating conditions (0.015 M SOA LC solution, 1 M NaCl HC solution, the resistance of 10 Ω, and flow velocity of 1.18 cm/s) as a function of the number of cell pairs. A single RED stack exhibited constant exergy of salinity gradient power at a constant flow rate. When the ratio of the salinity gradient between feed solutions was constant, the OCV and $P_{d,\ max}$ increased linearly as a function of the number of cell pairs. Increasing the number of cell pairs increased the electrical potential and affected the RED stack's hydraulic retention time and concentration polarization. Here, increasing the residence time allows more ions to be transported through the membranes to the opposite sides of the electrodes, thereby increasing the potential power generation in the cell [60]. In practice, however, determining the optimal number of membrane stacks associated with the highest RED system performance is not direct, but rather is influenced by the trade-off that exists between the high number of stacks responsible for maximum power generation and the associated costs such as manufacturing, installing (civil cost), and maintenance of the RED membranes. Furthermore, more detailed studies of the increasing effect of gross power and net specific energy as a function of the number of cell pairs of a single RED stack at a given constant flowrate revealed that this positive pattern does not increase infinitely, but converges to the limiting voltage value when the number of stacks exceeds 100 pairs [14]. This phenomenon persists due to the fact that as the number of cell pairs increases, the flow rate in the compartments per unit cell decreases, resulting in less entropy generation due to the mixing of solutions in the compartments, which in turn converges the gross power to a limiting value. Additionally, Nam et al. [40] evaluated RED stacks with 1000 pairs of cells under natural conditions. Their results showed that fouling and scaling of the membranes and electrodes caused lower power densities than expected.

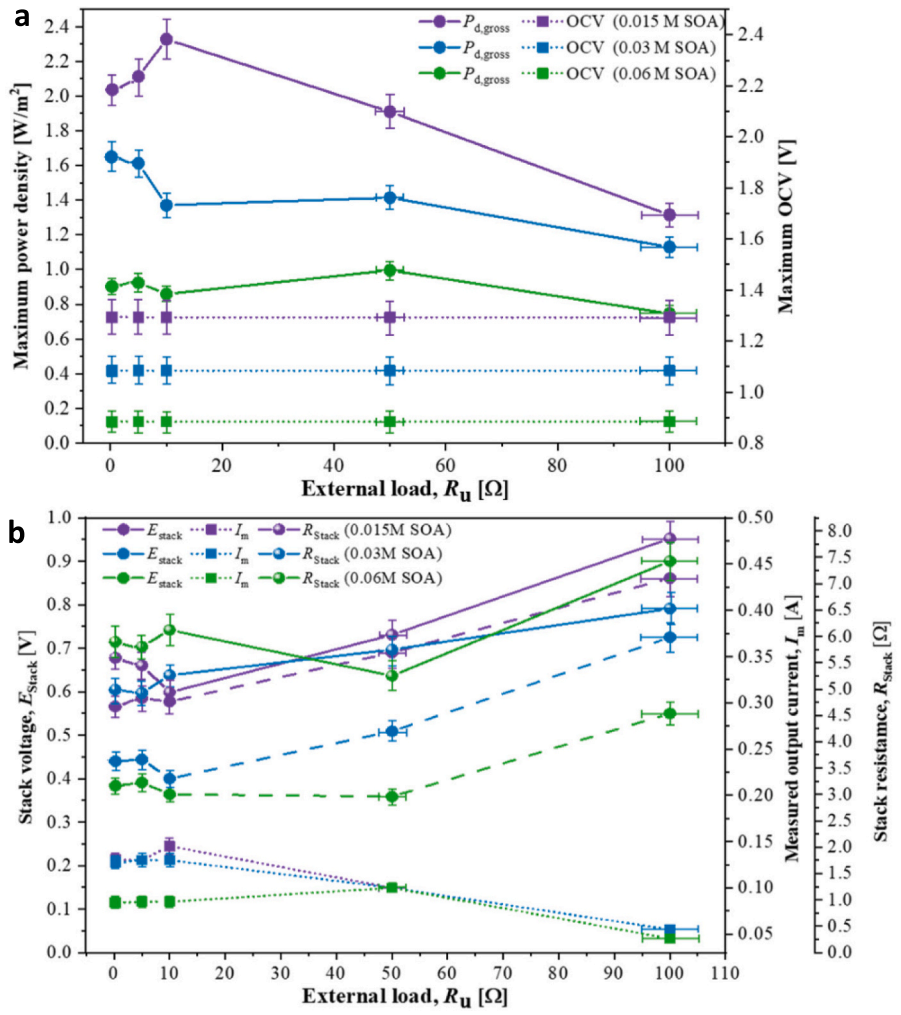

Fig. 9. Effect of the applied external loads on; (a) maximum acquired power density and OCV, (b) stack voltage, measured current, and stack resistance. The RED was operated using a recirculation flow mode in 1 M NaCl HC solution with a flow velocity of 1.18 m/s and 10 membrane cell pairs.

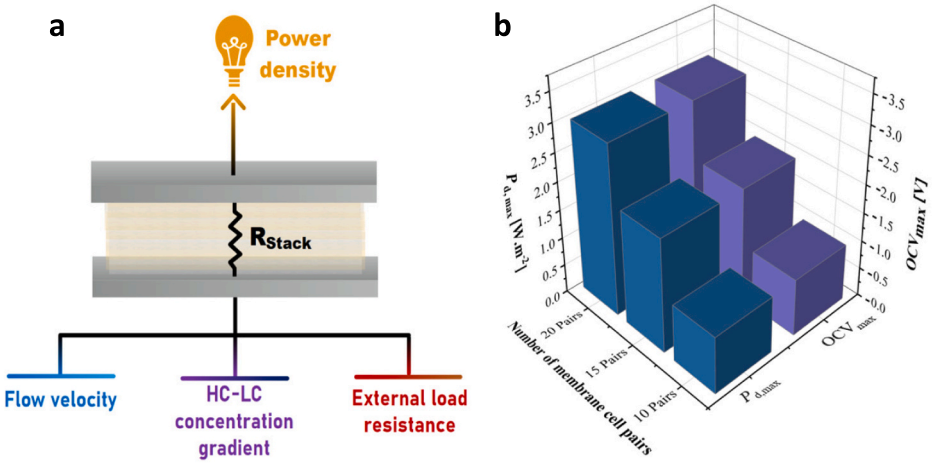

Fig. 10. (a) Schematic representation of the main variables contributing to the development of internal resistance inside the RED stack. (b) Effect of varying numbers of cell membrane pairs in RED at 1 M NaCl solution as HC solution and 0.015 M SOA solution as LC solution. Results were obtained by recirculating the feed solutions at 20 mL/min with 10 Ω of external load.

3.5. Feasibility of RED-FO hybrid system integration

This section relates to conducting a proof-of-the-concept experiment to verify that the RED outlet can be properly diluted in a FO system for fertigation purposes. Regarding the integration of the RED process with FO, the high and low salinity streams discharged from the RED system

are mixed and sent to the FO process as a DS after the salinity gradient between them is exhausted in a continuous flow in the RED system. Here, three different HC solutions (1 M, 1.25 M, and 1.5 M NaCl) were used to represent the various SWRO brine concentrations. The LC solution was fixed at the optimal 0.015 M SOA concentration obtained from the above experimental results. After thoroughly mixing, the resulting streams combined solutions were used as DS for the FO process. Fig. 11a graphically presents the experimental results obtained from the RED-FO hybrid process. The obtained results are consistent with the FO results shown elsewhere [61]. The experimental results presented here reveal similar patterns of improved patterns for both % water recovery and water flux with increasing DS concentration. However, looking at the initial and final TDS values of DS, the lowest combined concentration (1 M NaCl + 0.015 M SOA) experienced the highest dilution rate of ~25 %. In contrast, the dilution rates for the other FO runs with DS2 and DS3 were ~16 % and ~12 %, respectively. These outcomes indicate that the highest DS concentration requires more dilution for use in fertigation, suggesting that the lowest combined concentration is the optimal DS concentration for the FDFO process in the hybrid system. Nevertheless, further enhancement of the optimal DS1 should be considered to obtain a nutrient solution suitable for crop cultivation. For instance, the experimental results showed that the conductivities of all three DS outlet streams are significantly higher than the typical conductivity range of 1–4 mS/cm for nutrient solutions used in crop cultivation [62], making them unsuitable for direct fertigation. For example, Fig. 11b displays the material balance of the optimal scenario to achieve about 97 % of the dilution of DS, which corresponds to approximately a 4-fold dilution of the DS1 concentration. According to the FO principle, water will move across the membrane as long as the osmotic pressure difference between the FS and DS is maintained until equilibrium. Therefore, further dilution is required to improve the dilution rate of the DS side, which can be achieved by extending the operating time of the FO process. However, this approach is not practical as the continuous dilution of DS induces the dilutive internal concentration polarization (DICP) within the support layer (SL) of the FO membrane, as illustrated in Fig. 11c [63]. Subsequently, the driving force of FO is weakened due to the reduction in the osmotic pressure differential on both sides of the FO membrane, thus reducing water recovery and water flux. Therefore, further improvement of the FO process needs to be considered to enhance the dilution rate of the DS for direct fertigation while minimizing the loss of water flux. This involves fabricating the SL of the FO membrane with high porosity, less tortuosity, and ultra-thin thickness for minimum ICP effect. In addition, a hollow-fiber FO membrane [64,65] is an alternative approach for FO desalination because it has a larger active surface area than commercial flat-sheet TFC FO membranes. This case was demonstrated by Shon's study [66] that hollow-fiber FO membrane can dilute the concentrated DS from 119.06 mS/cm to 8.6 mS/cm. Another alternative to FO membrane materials is the pressure-assisted osmosis (PAO) process [66], which adds hydraulic pressure (~1–3 bar) to the FS side of the FO process. The PAO-FO system was able to dilute the DS to a level suitable for direct crop cultivation through the hydroponic system at an applied pressure of 2 bar, which helped in diluting the DS beyond the osmotic equilibrium point, which is not feasible under FO-mode operation alone. Thus, the PAO-FO process can eliminate an additional post-treatment process for the DS to be used for direct irrigation.

Fig. 12 shows the optimal operating parameters obtained from the RED process and the stream-by-stream integration with the FO process and related desired outcomes. Here, the inlet and outlet of the FS and DS accommodate the actual experimental solution conductivities retrieved using a (1 M NaCl + 0.015 M SOA) as DS in the FDFO system, where the conductivity of the draw inlet (RED outlet) is 36.6 mS/cm whereas that of the FS inlet is 7.6 mS/cm. By operating the FO system with these streams for 5 h, the DS outlet stream was diluted to 28.2 mS/cm, and the FS outlet stream was concentrated to 8.21 mS/cm.

Since the FO process is known to have the lowest energy requirement

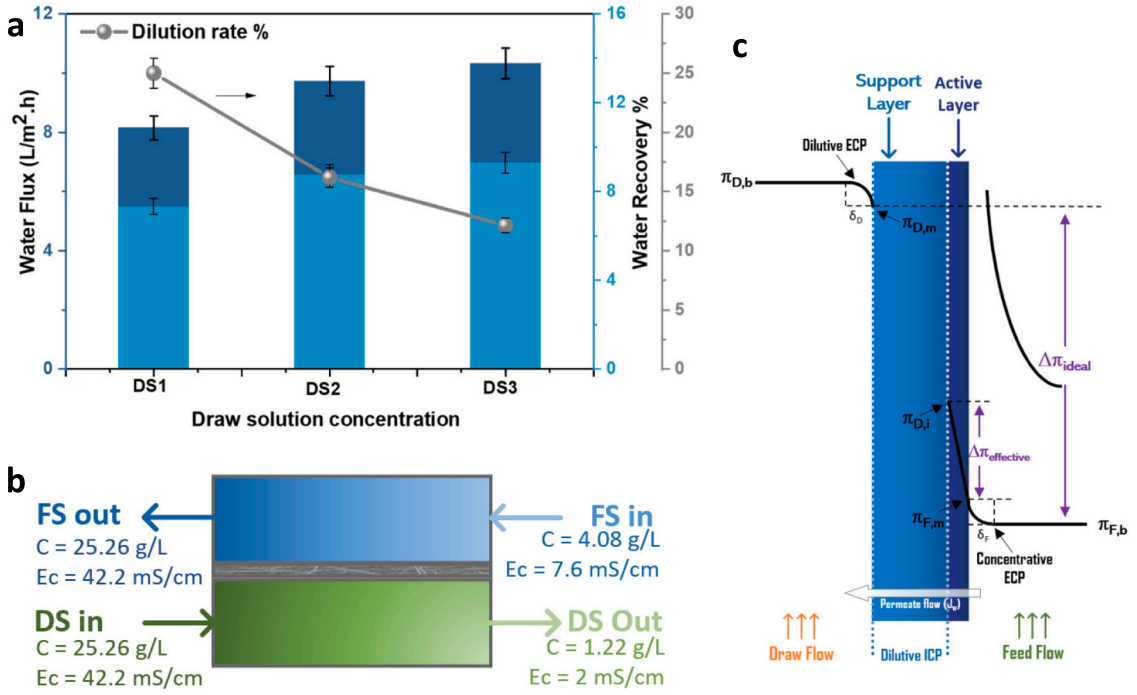

Fig. 11. (a) Performance of FO process using different concentrations of the RED effluent stream as DS (DS1: 1 M NaCl + 0.015 M SOA, DS2: 1.25 M NaCl + 0.015 M SOA and DS3: 1.5 M NaCl + 0.015 M SOA) operated at a fixed concentration of FS (0.1 M NaCl), circulation flow of 1 L/min and room temperature for 5 h. (b) Material balance of FO process to reach the desired final concentration of DS1 for direct fertigation. (c) External and internal concentration polarization in FO-mode (active layer facing FS), redrawn from [67].

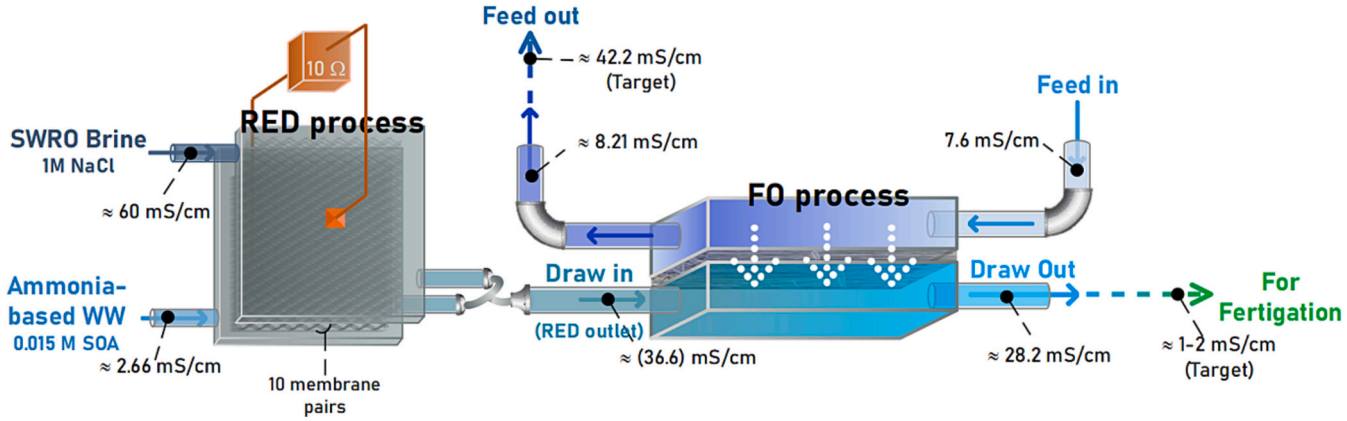

Fig. 12. Schematic diagram of RED-FO hybrid system for simultaneous blue energy harvest and direct fertigation.

among other membrane-based technologies [68], this study evaluated the feasibility of utilizing the RED blue energy as an energy source for pumping bulk solution in the FO process. The energy consumption of the FO process results from the pump power expressed as specific energy consumption (SEC), where P is the power required to transfer liquids, and V is denoted for the recovered volume expressed in Eq. (17) [69,70]. The FO's bench-scale setup consists of two pumps, each powered by 230 W at a maximum flow rate of 3.2 L/min. Therefore, we propose that the energy generated by the RED is supplied to these pumps. In this case, the maximum power generated by the RED was 0.24 W, estimated by multiplying the maximum power density (3.29 W/m^2) by the total membrane area of IEXMs (0.072 m^2). In the FO tests above, the SEC of the FO process operated at a fixed flow rate (1 L/min) was estimated to range from 1.08 kW/m^3 to 0.86 kW/m^3 for DS1-DS3, respectively. At the same time, the FO pump power [71] was estimated to be 0.16 W, which is determined by considering the head loss (H_m) through the hydraulic network and volumetric flowrate (Q), as displayed in Eq. (18). Under these conditions, the RED process can generate enough energy to supply two pumps operating at 1 L/min for the various DS combinations (DS1-D3).

$$E = \frac{P_{pump}}{V} \tag{17}$$

$$\boldsymbol{P_{pump} = H_m\, Q} \tag{18}$$

4. Conclusion

This study investigated the applicability of integrating a reverse electrodialysis (RED)-forward osmosis (FO) hybrid system in a fertilizer production plant that discharges ammonia-containing wastewater and SWRO brine. Here, the chemical potential energy of mixing a high salinity seawater reverse osmosis (SWRO) brine stream and a low salinity ammonia-based wastewater stream is converted into viable electrical power in the RED process. Simultaneously, the brackish level effluent stream from the RED process was passed to the FDFO processes as a draw solution for fertigation. Throughout the study, the effects of concentrate and dilute stream concentrations, compositions, and flow velocities variation on power generation from the RED process were investigated experimentally. In addition, the impact of flow mode alteration and the extent of the external load application was also examined in the RED cell. Finally, after optimizing the RED process parameters, this study investigated whether the effluent saline solution from the RED cell was suitable for its use as a draw solution in the subsequent FO system and whether there was a possibility of fertigation. The results of this study are summarized as follows.

- A comparison of single- and multi-component NaCl/SOA feed streams under identical operating conditions revealed that the composition of the feed streams plays a vital role in RED power generation. The combination of a NaCl solution (simulating high salinity SWRO brine) as the HC solution and an ammonium sulfate-based solution (simulating wastewater) as the LC solution was found to generate power in the 2.113–2.687 W/m^2 range in the RED system.
- Under similar operating conditions, increasing the salinity gradient between the LC and HC compartments increased the driving force for energy production. However, reducing the LC solution below 0.015 M or increasing the HC solution above 1.25 M degrades the performance of the RED system because of the internal resistance growth at very low LC concentrations and the reduced ion transport capacity of the membranes at elevated HC concentrations.
- Analysis of the recirculation mode of the RED feed solutions shows a trade-off between the total energy a single RED stack can generate and the amount of feed solution required obtaining it.
- The results show how increasing the flow velocity can slightly increase the gross power output. However, flow velocity exceeding a critical value (around 1.18 cm/s for the units and conditions investigated) results in unacceptable hydraulic pumping losses with negative net power output.
- With the variation of applied external loads in the RED system, the amount of power density attained is a virtue of the inverse relationship between the measured currents in the cell and the developed internal resistance. In addition, increasing the number of membrane cell pairs increases the potential and residence time of the solutions within the cell, directly affecting the power generated.
- A subsequent FO system using the mixed RED effluent (NaCl/SOA) as the draw solution and low salinity NaCl as feed solution showed a feasible dilution rate of NaCl/SOA effluent steam potentially usable in fertigation applications.

CRediT authorship contribution statement

Tasneem Elmakki: Methodology, Investigation, Writing-Original draft preparation.: **Sifani Zavahir**: Investigation, Resources, Formal Analysis.: **Mona Gulied:** Methodology, Investigation, Writing-Original draft preparation.: **Hazim Qiblawey:** Writing-Review & Editing, Validation.: **Bassim Hammadi:** Writing-Review & Editing, Validation.: **Majeda Khraisheh:** Writing-Review & Editing, Validation.: **Ho Kyong Shon:** Writing-Review & Editing, Validation.: **Hyunwoong Park:** Writing-Review & Editing, Curation, Validation.: **Dong Suk Han:** Conceptualization, Validation, Data Curation, Supervision, Funding acquisition.

Declaration of competing interest

The authors declare the following financial interests/personal relationships which may be considered as potential competing interests: Dong Suk Han reports financial support was provided by Qatar National Research Fund (QNRF). Dong Suk Han reports financial support was provided by Qatar Fertilizer Company (QAFCO).

Data availability

Data will be made available on request.

Acknowledgment

This publication was made possible by the Qatar National Research Fund (QNRF) (a member of the Qatar Foundation) under the NPRP grant (#NPRP13S-0202-200228) and supported by the Qatar Fertilizer Company (QAFCO) grant (QUEX-CAM-QAFCO-20/21-1). The findings achieved are solely the responsibility of the authors. H.P. is grateful to the National Research Foundation of Korea (2018R1A6A1A03024962 and 2019R1A2C2002602) and the Ministry of Trade, Industry, and Energy (MOTIE), Korea (2021-20015633) for financial support.

References

[1] J. Jang, Y. Kang, J.-H. Han, K. Jang, C.-M. Kim, I.S. Kim, Developments and future prospects of reverse electrodialysis for salinity gradient power generation: influence of ion exchange membranes and electrodes, Desalination 491 (2020), 114540.
[2] E. Jones, M. Qadir, M.T. van Vliet, V. Smakhtin, S.-M. Kang, The state of desalination and brine production: a global outlook, Sci. Total Environ. 657 (2019) 1343–1356.
[3] M. Khan, R.S. Al-Absi, M. Khraisheh, M.A. Al-Ghouti, A better understanding of seawater reverse osmosis brine: characterizations, uses, and energy requirements, Case Stud.Chem.Environ.Eng. 4 (2021), 100165.
[4] M. Bindels, J. Carvalho, C.B. Gonzalez, N. Brand, B. Nelemans, Techno-economic assessment of seawater reverse osmosis (SWRO) brine treatment with air gap membrane distillation (AGMD), Desalination 489 (2020), 114532.
[5] R.L. Stover, Seawater reverse osmosis with isobaric energy recovery devices, Desalination 203 (2007) 168–175.
[6] R.A. Tufa, S. Pawlowski, J. Veerman, K. Bouzek, E. Fontananova, G. Di Profio, S. Velizarov, J.G. Crespo, K. Nijmeijer, E. Curcio, Progress and prospects in reverse electrodialysis for salinity gradient energy conversion and storage, Appl. Energy 225 (2018) 290–331.
[7] J.W. Post, J. Veerman, H.V. Hamelers, G.J. Euverink, S.J. Metz, K. Nymeijer, C. J. Buisman, Salinity-gradient power: evaluation of pressure-retarded osmosis and reverse electrodialysis, J. Membr. Sci. 288 (2007) 218–230.
[8] M. Sharma, P.P. Das, A. Chakraborty, M.K. Purkait, Clean energy from salinity gradients using pressure retarded osmosis and reverse electrodialysis: a review, Sustain. Energy Technol. Assess. 49 (2022), 101687.
[9] J. Ju, Y. Choi, S. Lee, N. Jeong, Comparison of fouling characteristics between reverse electrodialysis (RED) and pressure retarded osmosis (PRO), Desalination 497 (2021), 114648.
[10] E. Farrell, M.I. Hassan, R.A. Tufa, A. Tuomiranta, A.H. Avci, A. Politano, E. Curcio, H.A. Arafat, Reverse electrodialysis powered greenhouse concept for water-and energy-self-sufficient agriculture, Appl. Energy 187 (2017) 390–409.
[11] V.M. Ortiz-Martínez, L. Gómez-Coma, C. Tristán, G. Pérez, M. Fallanza, A. Ortiz, R. Ibáñez, I. Ortiz, A comprehensive study on the effects of operation variables on reverse electrodialysis performance, Desalination 482 (2020), 114389.
[12] S. Pawlowski, J. Crespo, S. Velizarov, Sustainable power generation from salinity gradient energy by reverse electrodialysis, in: Electrokinetics Across Disciplines And Continents, Springer, 2016, pp. 57–80.
[13] X. Zhu, W. He, B.E. Logan, Influence of solution concentration and salt types on the performance of reverse electrodialysis cells, J. Membr. Sci. 494 (2015) 154–160.
[14] H. Kim, S. Yang, J. Choi, J.-O. Kim, N. Jeong, Optimization of the number of cell pairs to design efficient reverse electrodialysis stack, Desalination 497 (2021), 114676.
[15] J. Hu, S. Xu, X. Wu, D. Wu, D. Jin, Q. Leng, Multi-stage reverse electrodialysis: strategies to harvest salinity gradient energy, Energy Convers. Manag. 183 (2019) 803–815.
[16] J. Hu, S. Xu, X. Wu, S. Wang, X. Zhang, S. Yang, R. Xi, D. Wu, L. Xu, Experimental investigation on the performance of series control multi-stage reverse electrodialysis, Energy Convers. Manag. 204 (2020), 112284.
[17] A.H. Avci, D.A. Messana, S. Santoro, R.A. Tufa, E. Curcio, G. Di Profio, E. Fontananova, Energy harvesting from brines by reverse electrodialysis using nafion membranes, Membr. J. 10 (2020) 168.
[18] A. Zlotorowicz, R.V. Strand, O.S. Burheim, Ø. Wilhelmsen, S. Kjelstrup, The permselectivity and water transference number of ion exchange membranes in reverse electrodialysis, J. Membr. Sci. 523 (2017) 402–408.
[19] R. Long, B. Li, Z. Liu, W. Liu, Performance analysis of reverse electrodialysis stacks: channel geometry and flow rate optimization, Energy J. 158 (2018) 427–436.
[20] S. Mehdizadeh, M. Yasukawa, T. Abo, Y. Kakihana, M. Higa, Effect of spacer geometry on membrane and solution compartment resistances in reverse electrodialysis, J. Membr. Sci. 572 (2019) 271–280.
[21] H.-K. Kim, M.-S. Lee, S.-Y. Lee, Y.-W. Choi, N.-J. Jeong, C.-S. Kim, High power density of reverse electrodialysis with pore-filling ion exchange membranes and a high-open-area spacer, J. Mater. Chem. 3 (2015) 16302–16306.
[22] C. Simões, D. Pintossi, M. Saakes, Z. Borneman, W. Brilman, K. Nijmeijer, Electrode segmentation in reverse electrodialysis: improved power and energy efficiency, Desalination 492 (2020), 114604.
[23] O. Scialdone, C. Guarisco, S. Grispo, A. D'Angelo, A. Galia, Investigation of electrode material–redox couple systems for reverse electrodialysis processes. Part i: iron redox couples, J. Electroanal. Chem. 681 (2012) 66–75.
[24] D. Zhao, L.Y. Lee, S.L. Ong, P. Chowdhury, K.B. Siah, H.Y. Ng, Electrodialysis reversal for industrial reverse osmosis brine treatment, Sep. Purif. Technol. 213 (2019) 339–347.
[25] J. Choi, Y. Oh, S. Chae, S. Hong, Membrane capacitive deionization-reverse electrodialysis hybrid system for improving energy efficiency of reverse osmosis seawater desalination, Desalination 462 (2019) 19–28.
[26] F. Luo, Y. Wang, C. Jiang, B. Wu, H. Feng, T. Xu, A power free electrodialysis (PFED) for desalination, Desalination 404 (2017) 138–146.
[27] M. Bevacqua, A. Tamburini, M. Papapetrou, A. Cipollina, G. Micale, A. Piacentino, Reverse electrodialysis with nh4hco3-water systems for heat-to-power conversion, Energy J. 137 (2017) 1293–1307.
[28] J. Hu, S. Xu, X. Wu, D. Wu, D. Jin, P. Wang, L. Xu, Q. Leng, Exergy analysis for the multi-effect distillation-reverse electrodialysis heat engine, Desalination 467 (2019) 158–169.
[29] R.A. Tufa, Y. Noviello, G. Di Profio, F. Macedonio, A. Ali, E. Drioli, E. Fontananova, K. Bouzek, E. Curcio, Integrated membrane distillation-reverse electrodialysis system for energy-efficient seawater desalination, Appl. Energy 253 (2019), 113551.
[30] E. Mercer, C. Davey, D. Azzini, A.L. Eusebi, R. Tierney, L. Williams, Y. Jiang, A. Parker, A. Kolios, S. Tyrrel, Hybrid membrane distillation reverse electrodialysis configuration for water and energy recovery from human urine: an opportunity for off-grid decentralised sanitation, J. Membr. Sci. 584 (2019) 343–352.
[31] P. Ma, X. Hao, F. Proietto, A. Galia, O. Scialdone, Assisted reverse electrodialysis for CO2 electrochemical conversion and treatment of wastewater: a new approach towards more eco-friendly processes using salinity gradients, Electrochim. Acta 354 (2020), 136733.
[32] E. Jwa, K. Yoon, Y.S. Mok, J.-H. Oh, J. Han, Y.-C. Jeung, K.S. Hwang, H. Kim, N. Jeong, J.-Y. Nam, Enhanced electrochemical disinfection of domestic aquaculture wastewater with energy production in reverse electrodialysis, Aquac. Res. 548 (2022), 737554.
[33] X. Shiming, L. Qiang, J. Dongxu, W. Xi, X. Zhijie, W. Ping, W. Debing, D. Fujiang, Experimental investigation on dye wastewater treatment with reverse electrodialysis reactor powered by salinity gradient energy, Desalination 495 (2020), 114541.
[34] S. Xu, Q. Leng, X. Wu, Z. Xu, J. Hu, D. Wu, D. Jing, P. Wang, F. Dong, Influence of output current on decolorization efficiency of azo dye wastewater by a series system with multi-stage reverse electrodialysis reactors, Energy Convers. Manag. 228 (2021), 113639.
[35] R.A. Tufa, J. Hnát, M. Němeček, R. Kodým, E. Curcio, K. Bouzek, Hydrogen production from industrial wastewaters: an integrated reverse electrodialysis-water electrolysis energy system, J. Clean. Prod. 203 (2018) 418–426.
[36] S. Mehdizadeh, M. Yasukawa, T. Suzuki, M. Higa, Reverse electrodialysis for power generation using seawater/municipal wastewater: effect of coagulation pretreatment, Desalination 481 (2020), 114356.
[37] F. Volpin, Y.C. Woo, H. Kim, S. Freguia, N. Jeong, J.-S. Choi, J. Cho, S. Phuntsho, H.K. Shon, Energy recovery through reverse electrodialysis: harnessing the salinity gradient from the flushing of human urine, Water Res. 186 (2020), 116320.
[38] R. Kingsbury, F. Liu, S. Zhu, C. Boggs, M. Armstrong, D. Call, O. Coronell, Impact of natural organic matter and inorganic solutes on energy recovery from five real salinity gradients using reverse electrodialysis, J. Membr. Sci. 541 (2017) 621–632.
[39] A. D'Angelo, M. Tedesco, A. Cipollina, A. Galia, G. Micale, O. Scialdone, Reverse electrodialysis performed at pilot plant scale: evaluation of redox processes and simultaneous generation of electric energy and treatment of wastewater, Water Res. 125 (2017) 123–131.
[40] J.-Y. Nam, K.-S. Hwang, H.-C. Kim, H. Jeong, H. Kim, E. Jwa, S. Yang, J. Choi, C.-S. Kim, J.-H. Han, Assessing the behavior of the feed-water constituents of a pilot-scale 1000-cell-pair reverse electrodialysis with seawater and municipal wastewater effluent, Water Res. 148 (2019) 261–271.
[41] Y. Zhou, K. Zhao, C. Hu, H. Liu, Y. Wang, J. Qu, Electrochemical oxidation of ammonia accompanied with electricity generation based on reverse electrodialysis, Electrochim. Acta 269 (2018) 128–135.
[42] A. Beckinghausen, M. Odlare, E. Thorin, S. Schwede, From removal to recovery: an evaluation of nitrogen recovery techniques from wastewater, Appl. Energy 263 (2020), 114616.
[43] H. Abbasi, S.J. Khan, K. Manzoor, M. Adnan, Optimization of nutrient rich solution for direct fertigation using novel side stream anaerobic forward osmosis process to treat textile wastewater, J. Environ. Manag. 300 (2021), 113691.

[44] C.A. Quist-Jensen, F. Macedonio, E. Drioli, Membrane crystallization for salts recovery from brine—an experimental and theoretical analysis, Desalin. Water Treat. 57 (2016) 7593–7603.
[45] M. Tedesco, A. Cipollina, A. Tamburini, G. Micale, Towards 1 kw power production in a reverse electrodialysis pilot plant with saline waters and concentrated brines, J. Membr. Sci. 522 (2017) 226–236.
[46] T. Rijnaarts, E. Huerta, W. van Baak, K. Nijmeijer, Effect of divalent cations on red performance and cation exchange membrane selection to enhance power densities, Environ.Sci.Technol. 51 (2017) 13028–13035.
[47] T.-T. Nguyen, R.S. Adha, C. Lee, D.-H. Kim, I.S. Kim, Quantifying the influence of divalent cations mass transport on critical flux and organic fouling mechanism of forward osmosis membrane, Desalination 512 (2021), 115146.
[48] J. Ju, Y. Choi, S. Lee, C.-G. Park, T. Hwang, N. Jung, Comparison of pretreatment methods for salinity gradient power generation using reverse electrodialysis (red) systems, Membr. J. 12 (2022) 372.
[49] V.M. Bhandari, L.G. Sorokhaibam, V.V. Ranade, Industrial wastewater treatment for fertilizer industry—a case study, Desalin. Water Treat. 57 (2016) 27934–27944.
[50] V.V. Ranade, V.M. Bhandari, Industrial Wastewater Treatment, Recycling And Reuse, Butterworth-Heinemann, 2014.
[51] M. Tedesco, C. Scalici, D. Vaccari, A. Cipollina, A. Tamburini, G. Micale, Performance of the first reverse electrodialysis pilot plant for power production from saline waters and concentrated brines, J. Membr. Sci. 500 (2016) 33–45.
[52] H. Miyakawa, M. Maghram Al Shaiae, T.N. Green, Y. Ito, Y. Sugawara, M. Onishi, Y. Fusaoka, M. Farooque Ayumantakath, A. Saleh Al Amoudi, Reliable sea water RO operation with high water recovery and no-chlorine/no-SBS dosing in Arabian Gulf, Saudi Arabia, Membr. J. 11 (2021) 141.
[53] S. Pawlowski, J.G. Crespo, S. Velizarov, Pressure drop in reverse electrodialysis: experimental and modeling studies for stacks with variable number of cell pairs, J. Membr. Sci. 462 (2014) 96–111.
[54] H. Tian, Y. Wang, Y. Pei, J.C. Crittenden, Unique applications and improvements of reverse electrodialysis: a review and outlook, Appl. Energy 262 (2020), 114482.
[55] L. Jianbo, Z. Chen, L. Kai, Y. Li, K. Xiangqiang, Experimental study on salinity gradient energy recovery from desalination seawater based on red, Energy Convers. Manag. 244 (2021), 114475.
[56] D. Kim, K. Kwon, D.H. Kim, L. Li, Energy Generation Using Reverse Electrodialysis: Principles, Implementation, And Applications, Springer, 2019.
[57] Y. Zhang, X. Wu, S. Xu, Q. Leng, S. Wang, A serial system of multi-stage reverse electrodialysis stacks for hydrogen production, Energy Convers. Manag. 251 (2022), 114932.
[58] J. Veerman, M. Saakes, S. Metz, G. Harmsen, Reverse electrodialysis: performance of a stack with 50 cells on the mixing of sea and river water, J. Membr. Sci. 327 (2009) 136–144.
[59] M. Tedesco, E. Brauns, A. Cipollina, G. Micale, P. Modica, G. Russo, J. Helsen, Reverse electrodialysis with saline waters and concentrated brines: a laboratory investigation towards technology scale-up, J. Membr. Sci. 492 (2015) 9–20.
[60] F. Giacalone, P. Catrini, A. Tamburini, A. Cipollina, A. Piacentino, G. Micale, Exergy analysis of reverse electrodialysis, Energy Convers. Manag. 164 (2018) 588–602.
[61] S. Phuntsho, H. Park, D.S. Han, H.K. Shon, Sulfur-containing air pollutants as draw solution for fertilizer drawn forward osmosis desalination process for irrigation use, Desalination 424 (2017) 1–9.
[62] D.B. Hardeep Singh, in: Electrical Conductivity And pH Guide for Hydroponics, 2016.
[63] M. Gulied, F. Al Momani, M. Khraisheh, R. Bhosale, A. AlNouss, Influence of draw solution type and properties on the performance of forward osmosis process: energy consumption and sustainable water reuse, Chemosphere 233 (2019) 234–244.
[64] S. Phuntsho, J.E. Kim, M.A. Johir, S. Hong, Z. Li, N. Ghaffour, T. Leiknes, H. K. Shon, Fertiliser drawn forward osmosis process: pilot-scale desalination of mine impaired water for fertigation, J. Membr. Sci. 508 (2016) 22–31.
[65] F. Lotfi, S. Phuntsho, T. Majeed, K. Kim, D.S. Han, A. Abdel-Wahab, H.K. Shon, Thin film composite hollow fibre forward osmosis membrane module for the desalination of brackish groundwater for fertigation, Desalination 364 (2015) 108–118.
[66] L. Chekli, J.E. Kim, I. El Saliby, Y. Kim, S. Phuntsho, S. Li, N. Ghaffour, T. Leiknes, H.K. Shon, Fertilizer drawn forward osmosis process for sustainable water reuse to grow hydroponic lettuce using commercial nutrient solution, Sep. Purif. Technol. 181 (2017) 18–28.
[67] L. Ogletree, H. Du, R. Kommalapati, Shale oil & gas produced water treatment: opportunities and barriers for forward osmosis, 2021.
[68] M. Elimelech, W.A. Phillip, The future of seawater desalination: energy, technology, and the environment, Science 333 (2011) 712–717.
[69] S.P. Agashichev, K.N. Lootahb, Influence of temperature and permeate recovery on energy consumption of a reverse osmosis system, Desalination 154 (2003) 253–266.
[70] J.R. McCutcheon, M. Elimelech, Modeling water flux in forward osmosis: implications for improved membrane design, AIChE J. 53 (2007) 1736–1744.
[71] X. Xiang, S. Zou, Z. He, Energy consumption of water recovery from wastewater in a submerged forward osmosis system using commercial liquid fertilizer as a draw solute, Sep. Purif. Technol. 174 (2017) 432–438.